NASA SP-8049

NASA SPACE VEHICLE DESIGN CRITERIA (ENVIRONMENT)

THE EARTH'S IONOSPHERE

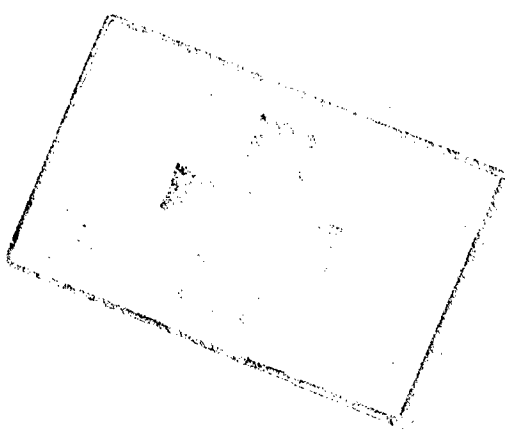

MARCH 1971

NATIONAL AERONAUTICS AND SPACE ADMINISTRATION

FOREWORD

NASA experience has indicated a need for uniform design criteria for space vehicles. Accordingly, criteria are being developed in the following areas of technology.

Environment
Structures
Guidance and Control
Chemical Propulsion

Individual components are issued as separate monographs as soon as they are completed. A list of all previously issued monographs in this series can be found at the back of this publication.

These monographs serve as guides to NASA design and mission planning. They are used to develop requirements for specific projects and also are cited as the applicable references in mission studies and in contracts for design and development of space vehicle systems.

This monograph was prepared by Exotech Inc., Washington, D.C., under the cognizance of the NASA Goddard Space Flight Center (GSFC). S.A. Mills of GSFC and M.T. Charak of NASA Headquarters were the program coordinators. R.G. Lyle and P.D. Stabekis of Exotech developed the monograph from a technical study report by M.A. Kasha of RCA Victor Company, Montreal, Canada, and published by Gordon and Breach, Science Publishers, under the title "The Ionosphere and its Interaction with Satellites."

An ad hoc committee at GSFC, chaired by S.J. Bauer, provided guidance in preparation of the technical study by RCA and the monograph by Exotech. Committee members were J.E. Jackson, E.J. Maier, and D.R. Burrowbridge.

Comments concerning the technical content of these monographs will be welcomed by the National Aeronautics and Space Administration, Goddard Space Flight Center, Systems Reliability Directorate, Greenbelt, Maryland 20771.

March 1971

CONTENTS

THE EARTH'S IONOSPHERE

1. INTRODUCTION

The ionosphere is that region of the upper atmosphere where an appreciable amount of ionization exists. This region extends outward from altitudes of approximately 60 km until it merges with the plasma of interplanetary space.

The ionosphere is of concern to space vehicle designers because of the effects of spacecraft interaction with the electrically active medium and because of the influence of the ionosphere on mission communications, guidance, and tracking. Specifically, the ionosphere may affect frequency selection and design of receivers, transmitters, and antennas. In addition the flow of charge between the plasma and the spacecraft represents a leakage current to exposed conductors which may lead to electrical breakdown of normally non-conducting paths.

The interaction of the spacecraft and medium must be taken into account in the design of experiments having the purpose of taking measurements within the ionosphere. These interactions include formation of wakes by passage of the spacecraft through the medium, generation of large electrical potentials by long antennas and booms, and formation of plasma sheaths around the spacecraft which can isolate it from the ambient medium. Sheaths can affect results of direct measurement experiments such as Langmuir probes, and experiments mounted on booms. In addition, the electric potential acquired by the spacecraft usually serves as a reference for onboard experiments of this type.

This monograph describes the characteristics of the Earth's ionosphere which must be taken into account in space vehicle design. They include electron density and temperature, the neutral component, ionic composition, and plasma temperature. In addition, derived functions are given which are useful for analyzing the interaction of the spacecraft and ionospheric medium.

Two other monographs in this series (refs. 1 and 2) describe other aspects of the Earth's upper atmosphere. SP-8021 gives density and composition models of the Earth's atmosphere from 120 to 1000 km, and SP-8017 gives models of the Earth's magnetic field.

2. STATE OF THE ART

2.1 Background

2.1.1 Collection Methods

Existence of conducting layers in the atmosphere was apparent from the discovery that radio signal propagation did not conform to the predicted line-of-sight path. The reflective

property of the ionosphere for wavelengths greater than approximately 15 meters is of great practical importance since it makes possible long range communication by signals which would be otherwise lost in space. Until the last decade, the principal means of investigating the ionosphere had been radio sounding techniques from ground based stations. Although these studies were accurate, they were limited to altitudes generally below 300 km and to the geographical region of the sounding station. Incoherent backscatter stations and satellites such as the "topside sounder" spacecraft have made possible synoptic coverage to much greater altitudes.

2.1.2 Basic Concepts

The ionization of the upper atmosphere is the result of solar radiation and cosmic rays interacting with the atmosphere to produce a plasma consisting of (usually) equal concentrations of positively and negatively charged particles. The plasma remains in a state of dynamic equilibrium because the loss of charged particles through recombination is balanced by the creation of new particles. Because the prime source of energy for the ionosphere is the Sun, the parameters defining the ionosphere vary diurnally, seasonally, and with the solar cycle. Geographical variations from anomalies in the Earth's magnetic field also exist.

At equatorial and middle latitudes, the terrestrial magnetic field tends to "hold" ionospheric particles within a magnetic shell at an average geocentric distance ρ, given approximately by $\rho = 4\,R_E\,\mathrm{Cos}^2\lambda$ where R_E is the earth's radius and λ is the geographic latitude. Electron densities at this "boundary" (plasmapause) are of the order of 100 electrons cm^{-3}. Beyond the plasmapause, the ionosphere has electron densities of at least one order of magnitude smaller and is linked with the outer magnetosphere. In the polar regions the ionospheric particles are not "held" by the terrestrial magnetic field but escape via the polar wind mechanism. Consequently, electron densities are typical of those beyond the plasmapause and the ionosphere is linked with the outer magnetosphere.

A general discussion of the ionosphere is possible only in terms of the limit of variations or ranges, i.e., daytime solar maximum and solar minimum conditions and nighttime solar maximum and solar minimum conditions. Thus models of this environment are generally in the form of solar maximum and solar minimum limits. The basic parameters used to define the ionosphere are electron density, neutral and ion composition, density, and temperature. Of these parameters, the electron density has been measured more extensively. The ion composition and ionospheric temperature are derived largely from satellite and rocket data, and the neutral composition is usually based on standard theoretical models. Models of the ionosphere that are suitable for spacecraft design considerations present profiles of these parameters with altitude.

The variations of ionospheric parameters with altitude are of sufficient magnitude below 1000 km to permit the identification of distinct regions. Above 1000 km, the changes in those parameters with altitude are much more gradual. For convenience of presentation and discussion, this monograph considers the ionosphere in two parts, divided at an altitude of 1000 km.

2.2 The Ionosphere Below 1000 km

Three regions have been identified as prominent features of the structure of the lower ionosphere during the daytime. In order of increasing altitude and increasing ion concentration they are the D, E, and F regions. There are large diurnal effects which occur in this part of the ionosphere. At nighttime, the D region virtually disappears and a depression in electron concentration occurs between the E and F regions.

The D region is the lowest ionospheric region and has an approximate altitude range from 60 to 85 km. The predominant ionizing agent is Lyman alpha radiation with cosmic rays contributing in the lower altitudes. Nitric oxide (NO^+) and oxygen (O_2^+) are the principal ionic constituents together with heavy ion complexes involving water vapor. The D region has the lowest electron density concentration of the three regions with a maximum of 10^3 electrons/cm^3 near 80 km.

The approximate altitude range of the E region is from 85 to 140 km. Ultraviolet and soft x-radiation are the principal ionizing agents in this region. The predominant ionic constituents are NO^+ and O_2^+ The electron concentration in the E region ranges from approximately 10^5 electrons/cm^3 during solar minimum to a value 50 percent larger during solar maximum.

The F region has an approximate altitude range from 140 to 1000 km and in daytime has two divisions, F_1 and F_2. The solar spectrum in the wavelength range from 200 Å to 900 Å is the principal ionizing agent in this region. The two divisions or density peaks occur because the degree of ionization and recombination falls off with decreasing altitude at different rates. The F_1 region is associated with the ion production peak occurring in the vicinity of 150 km. The F_1 region disappears at night as the concentration of electrons decreases above the E region. The F_2 region is associated with the peak in the electron density distribution which varies with time of day, season, solar cycle, and latitude. It usually lies within the region from 200 to 400 km. The predominant ions near the low altitude boundary are mainly NO^+ and O_2^+; with increasing altitude a gradual transition occurs until at the upper boundary O^+ becomes the principal ion.

The section of ionosphere above the peak of the F_2 region commonly is referred to as the topside ionosphere. Information on the topside ionosphere is obtained mainly through satellite measurements and the incoherent backscatter radar technique.

2.3 The Ionosphere Above 1000 km

The ionosphere above 1000 km includes the upper portion of the topside ionosphere and the region of the near-Earth plasma (or outer ionosphere) extending to altitudes of the order of 3 to 4.5 earth's radii (R_0). From this altitude to about 10 R_0 is the region of transition to the interplanetary medium (ref. 3).

Most information on the outer ionosphere has come through experimental research with the aid of whistlers (RF electromagnetic signals generated by some lightning discharges)

although in situ measurements by satellites also have provided useful results. The data indicate a steady decrease in electron concentration with increasing altitude until a rapid and abrupt decrease occurs at altitudes of 15 to 25 thousand kilometers above the magnetic equator. This decrease in electron concentration is called the "knee" or plasmapause.

The predominant ions in the outer ionosphere vary with altitude. In the lowest part of the region atomic oxygen (O^+) predominates whereas atomic hydrogen (H^+) is the main constituent above 2000 km (protonosphere).

A detailed examination of the outer ionosphere is presented in reference 3.

2.4 Ionospheric Parameters

2.4.1 Electron Densities

The density of electrons in the ionosphere varies geographically, diurnally, seasonally, and with solar activity. It is not yet possible, however, to produce models of the electron density distribution which show all these variations because of the limited number of observations. Available information is provided mainly by vertical incidence sounders and rockets and by satellites.

Below the peak of the F_2 region the electron density increases with altitude. Above this region, measurements (made primarily with topside sounders and incoherent backscatter radars) indicate a rather smooth and slow decrease in electron concentration with increasing altitude. In the region of the knee (where measurements have been made by whistlers and satellites), a very rapid decrease in electron concentration occurs. This decrease occurs even during the periods of relatively weak magnetic disturbances.

Details of experimental results and some theoretical discussions may be found in references 4 and 5. The "knee" (plasmapause) phenomenon has been analyzed by observation of whistler dispersion and certain types of micropulsations (refs. 6, 7, 8 and 9) as well as by direct measurements by satellites. Variations of the position of the knee because of magnetic activity are treated in references 6, 7, and 10.

2.4.2 Neutral Component

The upper atmosphere is not fully ionized. The part of the upper atmosphere which is not ionized is referred to as the neutral component. For altitudes up to 1000 km, the neutral component is represented by two models: one for altitudes below 120 km and the other for the region above 120 km. Both models provide atmospheric density, chemical composition, temperature, molecular mass, and density scale height. They are presented in detail in references 11 and 1.

For altitudes above 1000 km, the neutral atmosphere is almost exclusively hydrogen. Theoretical models and some experimental evidence are available for the hydrogen concentration (refs. 12 and 13). The theoretical model presented in this monograph covers the altitude range between 1000 and 20 000 km for various neutral component temperatures. For the region above 20 000 km some experimental evidence is included.

2.4.3 Ionic Composition

In the lower regions of the ionosphere, NO^+ and O_2^+ predominate with O^+ becoming the main ionic constituent in the higher part of the F region. A transition between a predominantly O^+ ionosphere to one predominantly of H^+ occurs in moving upward in the topside ionosphere. Helium is never a predominant ion species. It is, however, a minor constituent at all times; its maximum density is 15 per cent of the total at about 450 km (ref. 14). A detailed discussion of the ionic composition below 1000 km is in references 14 and 15, and the theory for the composition of this region is in reference 16.

Above 1000 km, the ionic composition is predominantly H^+; it becomes almost exclusively H^+ above 2,800 km. The only other component of interest is He^+ with a concentration of about 1 to 4 per cent of the hydrogen concentration (ref. 17). The concentration of hydrogen ions is deduced from proton whistler observations by the Alouette 1 and Injun 3 satellites (refs. 18 and 19). Concentrations of ions other than hydrogen are derived from incoherent backscatter data (ref. 20). Observations indicate that the concentration of hydrogen ions increases in winter and that the nighttime summer results may be applied to daytime winter conditions. The values then merge with those below 1000 km.

2.4.4 Ionospheric Temperature

The temperature profile of the ionosphere above the E region has been obtained with measurements by sounding rockets and satellites and backscatter sounders. The temperature of the ionosphere depends on the balance between the various heating and cooling processes in the ionosphere and the diurnal and seasonal variation of this balance. The daytime temperature of the ionospheric electrons in the F_1 region is generally larger than the ambient gas temperature by a factor of two (ref. 21). This results from the relative efficiency of the ambient electrons in removing the excess kinetic energy from the continually released energetic photoelectrons and the relatively small number of electrons to share such energy. The resulting hot electron gas is cooled mainly by collisions with neutral particles at altitudes below about 250 km and by collisions with ions at higher altitudes. The temperature of the ions approaches that of the electrons above 600 km with both exceeding the neutral gas temperature (ref. 22).

The model presented herein is based on experimental results for altitudes below 1000 km (ref. 23).

Satellites have provided some measurements which are presented in references 3 and 24, and the theory of ionospheric temperature is considered in reference 25. Temperature

measurements made by the IMP 1 spacecraft in the region from 2 to 5 R_E show that the electron temperature, T_e, is approximately proportional to the square of the radial distance, L, from the Earth (ref. 24). For this monograph, the value of 2.4 for the power of L is used to join lower altitude daytime temperature to data obtained from the OGO-1 satellite. The value of 1.9 was used as the power of L to match nighttime values of T_e with the low temperature readings of reference 24.

2.5 Spacecraft Interaction with the Ionosphere

2.5.1 Spacecraft Potential

A spacecraft moving through the ionospheric plasma will gather charge as a result of its contact with both positive and negative charges. In a state of equilibrium the spacecraft will assume a potential sufficiently negative to equalize the flow of ions and electrons. This potential depends upon the temperature of the ambient plasma, the relative spacecraft motion, the electron density, the electrostatic fields surrounding electrically active surfaces, the incident flux of ultraviolet radiation and energetic particles, and the intentional ejection of charge by onboard equipment.

The spacecraft potential is important because it generally is used as a potential reference for onboard experiments. In this case, the spacecraft vehicle potential is assumed to be constant, and any variation in its value appears as an inaccuracy in the final experimental result. This dependence on the spacecraft potential has been reported and related inaccuracies in experimental results have been noted (refs. 26, 27, and 28). Equations used to evaluate the spacecraft potential are presented in appendix A.

2.5.2 Plasma Sheaths

The potential of the spacecraft is usually different from that of the ambient plasma, and as a result the spacecraft tends to be surrounded by a plasma sheath. There are three different classes of plasma sheaths: (a) the stationary sheath, (b) the wake, and (c) the specialized sheaths formed by exposure to direct voltages induced by R-F or $\overline{V} \times \overline{B}$ (sec. 2.5.3). It should be noted, however, that the spacecraft plasma sheath usually is a compound of all three forms unless special measures have been taken to eliminate certain of them.

The stationary sheath is formed around a body placed in a plasma. Theoretical analyses usually assume that the body is spherical and the sheath is of dimension considerably larger than the plasma Debye length, λ_D (defined as $6.9\ [T_e/N_e]^{1/2}$ where T_e is the electron temperature in °K and N_e the electron density in cm^{-3}). However, the sheath is considered smaller than the mean free path of the particles. These conditions permit collisionless treatment of the plasma in such analyses.

The sheath effects associated with the presence of an R-F signal on an antenna strongly depend on the relationship between its frequency and the local plasma frequency. In

general, an R-F signal can cause the formation of quite extensive sheaths around an antenna which may disturb direct measurement experiments.

2.5.3 $\overline{V} \times \overline{B}$ Effects

When a conductor moves through a magnetic field, an electric field is developed across the conductor according to the relationship,

$$\overline{E} = \overline{V} \times \overline{B}$$

where

$\overline{E}$ = the electric field produced

$\overline{V}$ = the velocity vector of the conductor

$\overline{B}$ = the magnetic field

In the case of the spacecraft's interaction with the environment, the magnetic field is that of the Earth, and the conductor is the metallic skin or appendages of the spacecraft.

If good coupling exists between the spacecraft and the plasma, an appreciable current will flow under the influence of the induced field. The energy of the spacecraft can be radiated away by resistive heating, and the net effect is equivalent to a loss of energy by a drag mechanism. This drag effect of the $\overline{V} \times \overline{B}$ mechanism is treated in reference 29. It concludes that the drag is proportional to the cube of the spacecraft's characteristic dimension and may exceed the mass drag for spacecraft larger than 50 m in diameter above an altitude of 1200 km. However, reference 30 treats only spherical spacecraft whereas small spacecraft may have very large booms or antennas so that the total potential difference induced may be considerable (this potential is $(\overline{V} \times \overline{B}) \cdot \overline{L}$ where $\overline{L}$ is the vector length of a boom or antenna). This problem has been further studied in references 30 through 33. The total voltage developed can be decreased by breaking up the length, L, with a capacitor, i.e., capacitively coupling the antenna to the spacecraft body (ref. 34).

Another $\overline{V} \times \overline{B}$ effect is the formation of an induced plasma sheath associated with a large potential of perhaps tens of volts. This sheath varies as the spacecraft spins and thus changes orientation with respect to the magnetic field. Therefore, it can have unfortunate effects on experiments mounted on the spacecraft such as Langmuir probes measuring ambient densities and temperatures.

2.5.4 The Spacecraft Wake

The wake, which is a distorted sheath formed by the relative motion between the spacecraft and the plasma, extends many spacecraft diameters downstream. Immediately behind the spacecraft there is a region of high negative potential followed by an ion-focusing or concentration. Indications are that from this concentration an ion density enhancement extends downstream as a V wave analogous to a Mach cone. This enhancement is not

attached to the spacecraft but commences at a number of body radii downstream equal to the Mach number. References 35 through 37 examine the phenomenon of wake formation and include graphical representations in the form of contour maps and sectional pictures. Figure 1 illustrates the disturbed wake region on the basis of a rough combination of data from the above references.

2.5.5 Wave Phenomena

The electromagnetic waves in the plasma can affect adversely the receiving and radiating properties of antennas on a spacecraft. Cold plasma wave phenomena covering a range of frequencies from high to ultra-low are presented in appendix B. Appendix C discusses the effects of the ionospheric plasma on spacecraft antennas and presents techniques for giving quantitative results when the plasma effects are relatively small.

2.5.6 The Plasma as a Conductor

The normal thermal motions of the ions and electrons in the ionosphere represent small, but sometimes significant, electrical currents. Because of the low energies of the particles, they are easily attracted or repelled by terminals, wiring, and various types of electrodes on the outside of the spacecraft which are at some applied potential with respect to the spacecraft surface. These exposed conductors act as Langmuir probes in their interception of the plasma current.* For a Langmuir probe, the current-voltage response of an exposed conductor with an applied potential depends on the shape of the conductor, the value of the potential, and the characteristics of the local ionosphere and magnetic field. In general, it is difficult to determine accurately the leakage current between an exposed conductor and the plasma. Qualitatively, however, the current density arising from ions or electrons is represented by

$$I = \pm AenV_T \text{ amperes/cm}^2$$

where e is the electronic charge, n is the ambient electron (or ion) density, V_T is the thermal velocity of the ambient electrons (or ions), and A is an enhancement factor which is generally in the range 0.1 to 100. In the case of high exposed potentials (voltages greater than 50), the acceleration of the ambient particles in the electric field of the exposed potential may be sufficient to ionize the ambient medium further. This can have the effect of producing corona discharges or insulation breakdown across regions which were non-conducting in a simple vacuum environment. Several cases of electrical problems on spacecrafts in the ionosphere have been discussed by Street, et al.**

*Loeb, L. B.: Basic Processes of Gaseous Electronics. Univ. of Calif. Press (Berkeley), 1955.

**Street, H. W. L.; et al.: High Voltage Breakdown Problems in Scientific Satellites. NASA TM X-55497, Feb. 1966.

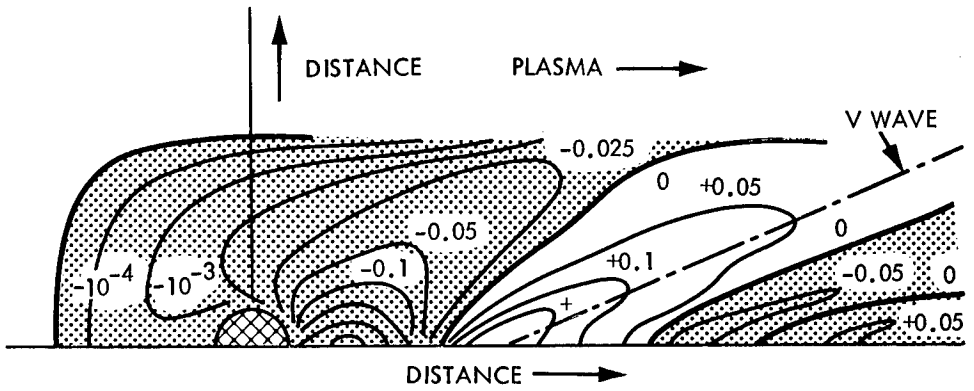

EQUIPOTENTIAL CONTOURS, ALL UNITS ARBITRARY

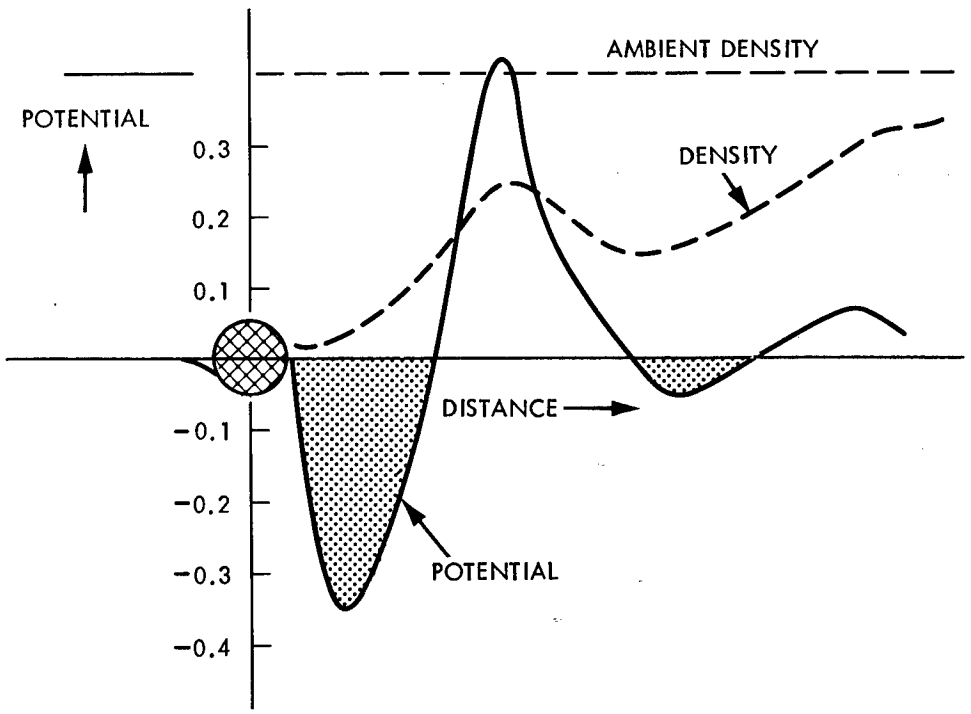

SECTION THROUGH WAKE PARALLEL TO FLOW, ALL UNITS ARBITRARY

Figure 1 - Wake region of spacecraft in plasma (ref. 38).

2.6 Derived Functions

Thermal velocities, plasma frequency, Debye length, collision frequencies, cyclotron frequencies, particle flux, Alfven velocity, lower hybrid frequency, and $\overline{V} \times \overline{B}$ field are functions obtained from various combinations of the primary parameters. These functions are essential in the design of experiments and communication systems.

Thermal velocities are those with which the ions and electrons move by virtue of their thermal energy. When the spacecraft velocity is much greater than the ion thermal velocity, the ions appear stationary; this is of considerable importance in determining the collection of charge by a spacecraft. Thus the thermal velocities may serve as a criteria for determining whether or not the thermal motion of particles can be neglected.

The plasma frequency, f_p, is a resonant frequency of the plasma. For practical purposes, it is that frequency below which electromagnetic radiation cannot be transmitted by the plasma except under the special circumstances associated with the plasma containing an embedded magnetic field (i.e., magnetoplasma).

The Debye length can be considered as a criterion for the application of plasma theories. In considering the collection of charge by a probe of dimensions much smaller than the plasma Debye length, microscopic or particle techniques must be used. For dimensions larger than the Debye length, it is possible to use continuous flow considerations and theories.

The collision and cyclotron frequencies, ν_e and f_H, respectively, are important to considerations of electromagnetic wave propagation through the plasma because they represent resonant conditions. The cyclotron frequency is applicable to magnetoplasmas only, i.e., plasmas with an embedded static magnetic field. In the ionosphere, the magnetic field is that of the Earth. In such case, under the influence of some applied force such as an electric field, a charged particle does not drift in a straight line but in a spiral centered about a magnetic field line. The radius of the spiral is known as the Larmor radius, $r_H = V_{Te}/\omega_H$ where V_{Te} is the electron thermal velocity and ω_H is the angular cyclotron (gyro) frequency.

The (thermal) particle flux is generally governed by the thermal velocities and the velocity of the spacecraft. Measurement of the particle flux is essential for scientific spacecraft carrying experimental sensors.

The Alfven velocity, V_A, and the lower hybrid frequency, f_{LH}, are specialized functions arising from a consideration of the wave modes of a plasma. The Alfven velocity is the velocity of the low frequency nondispersive waves associated with a magnetoplasma and is given by $V_A = B_o/\sqrt{\mu_o \rho_s}$ where B_o is the magnetic field induction, μ_o is the permeability of free space, and ρ_s is the mass density. The lower hybrid frequency represents the boundary between ion and electron effects and is given by $f_{LH} = [\overline{F}_H f_H/(1 + f_H^2/f_p^2)]^{1/2}$ where $\overline{F}_H$ is the average ion cyclotron frequency, and f_p is the plasma frequency. The practical importance of the Alfven velocity and the lower hybrid frequency becomes appar-

ent in the analysis of wave experiments carried in satellites wherein parameters depending on such functions may appear as resonances or apparently spurious signals.

The $\overline{V} \times \overline{B}$ field is the electric field produced by a conductor moving through a magnetic field and is of primary importance to phenomena such as the plasma sheaths and the drag effect (secs. 2.5.2 and 2.5.3).

3. CRITERIA

The characteristics of the Earth's ionosphere presented here should be considered in the design of space vehicles, their systems, experiments, and instrumentation. The quantitative information in this section is most representative of mean values for the mid-latitude region of the ionosphere (between 20° and 40° geomagnetic latitude).

3.1 Electron Density

Typical mid-latitude electron density profiles for the ionosphere below 1000 km are presented in figures 2 and 3. Variations with latitude are shown in figure 4. If greater accuracy is required, the tabulated values of electron density in references 40 and 41 should be consulted; these references cover both the mid-latitude and polar ionosphere. Profiles for the ionosphere above 1000 km are presented in figure 5. The solar maximum curve is an average daytime profile; the solar minimum profile up to the knee region is derived from incoherent scatter data (ref. 4), and a theoretical model is described in reference 5.

3.2 Neutral Component

The neutral atmosphere below 1000 km on the basis of an exospheric temperature of 1000°K is presented in figure 6. Models using temperatures other than 1000°K as well as calculations of exospheric temperature based on solar activity, diurnal variation, and geomagnetic activity are given in reference 11. The neutral hydrogen concentration above 1000 km is presented in figure 7.

3.3 Ionic Composition

The number variation of ionic composition in the lower ionosphere in daytime is presented in figure 8. The percentage variation of ionic composition is presented in figure 9. This information was deduced from proton whistler observations (refs. 19 and 20) on the Alouette 1 and Injun 3 satellites and from incoherent backscatter data (ref. 21). Averaging the various percentage concentrations with respect to mass yields night and day profiles of average ion mass.

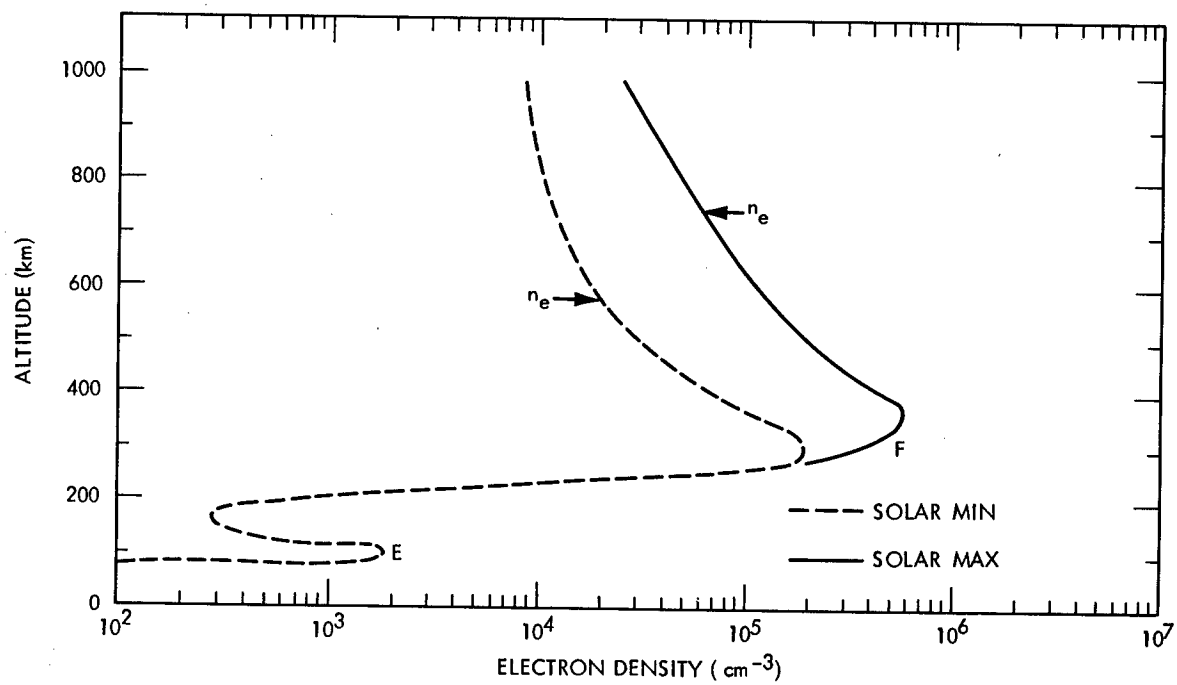

Figure 2 - Ionospheric electron concentration - nighttime (ref. 38).

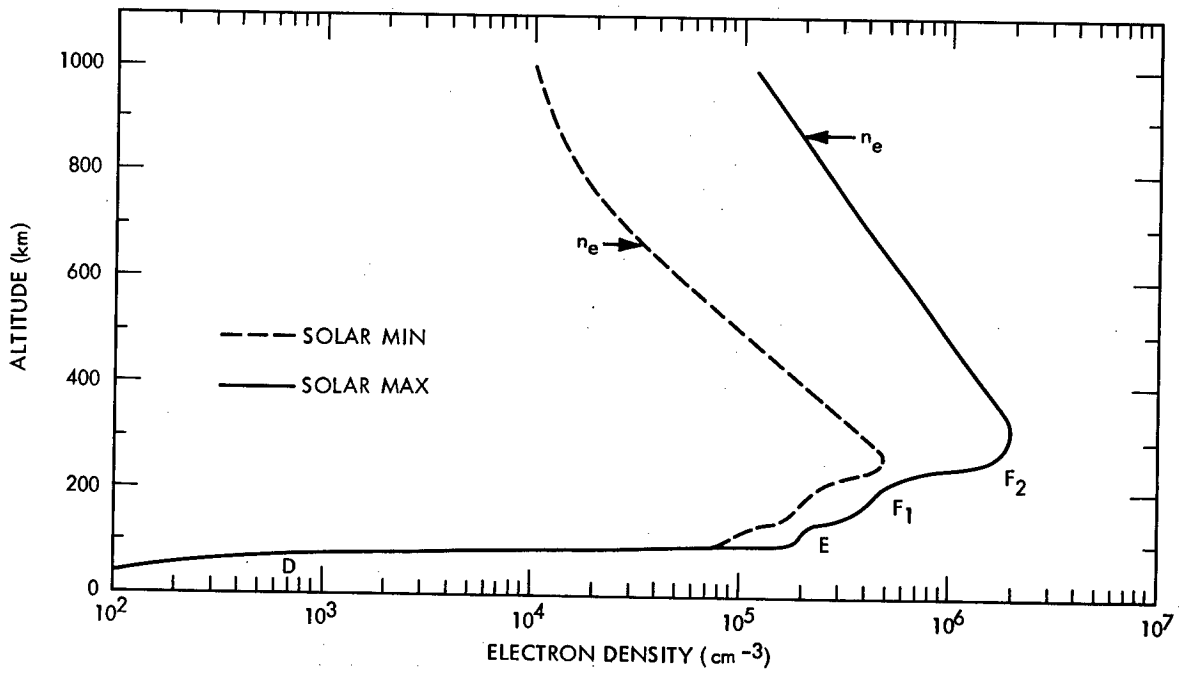

Figure 3 - Ionospheric electron concentration - daytime (ref. 38).

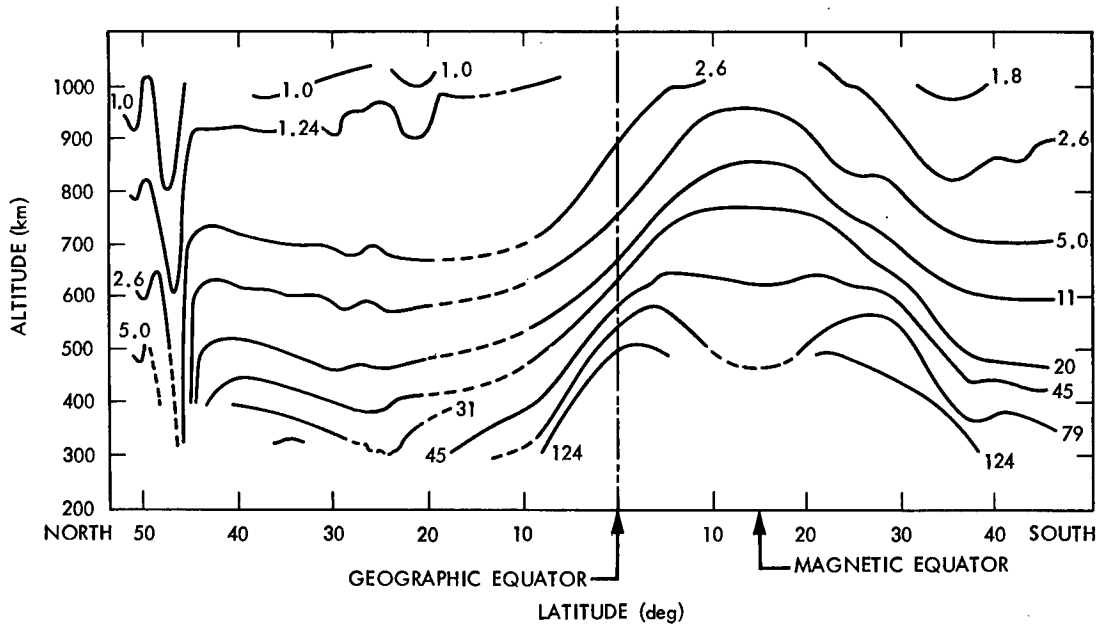

Figure 4 - Daytime contours of equal electron density in the orbital plane of an Alouette Satellite. Density units of 10^4 electrons cm^{-3} (ref. 39).

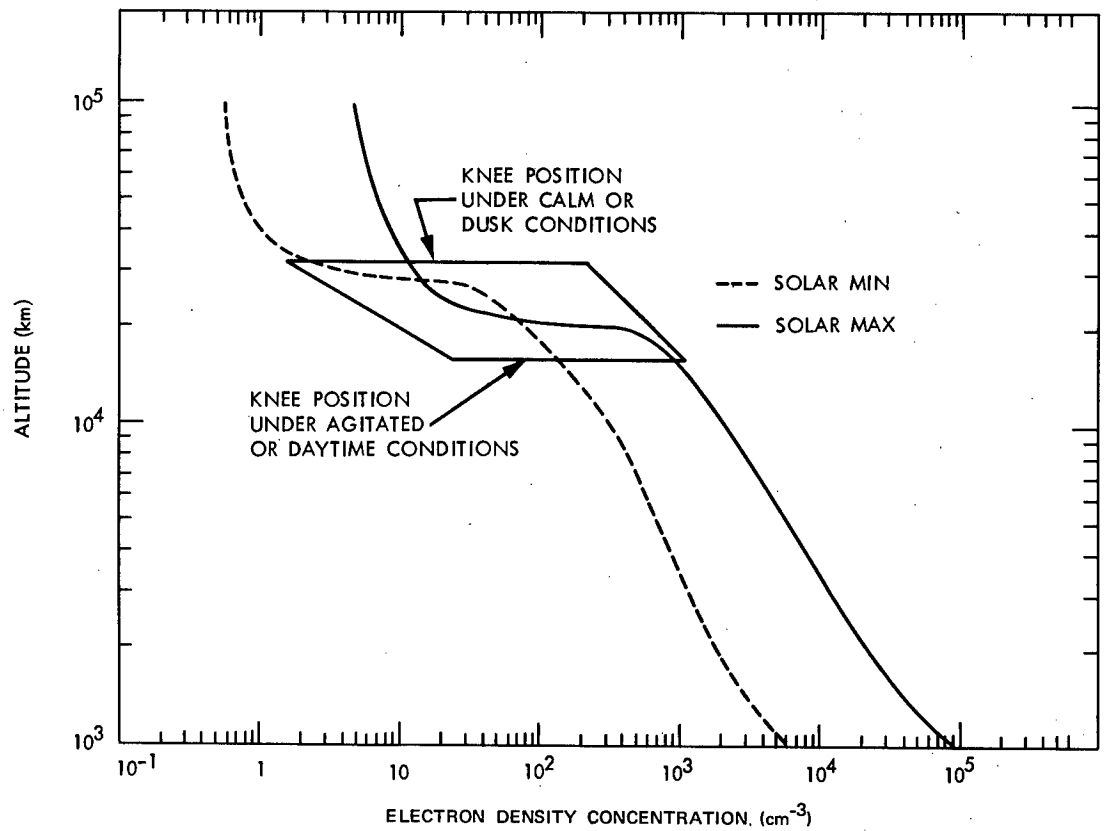

Figure 5 - Models of electron density profiles in the equatorial plane under solar sunspot extreme conditions. The position of the knee or abrupt decrease in density is variable within the box as indicated (ref. 38).

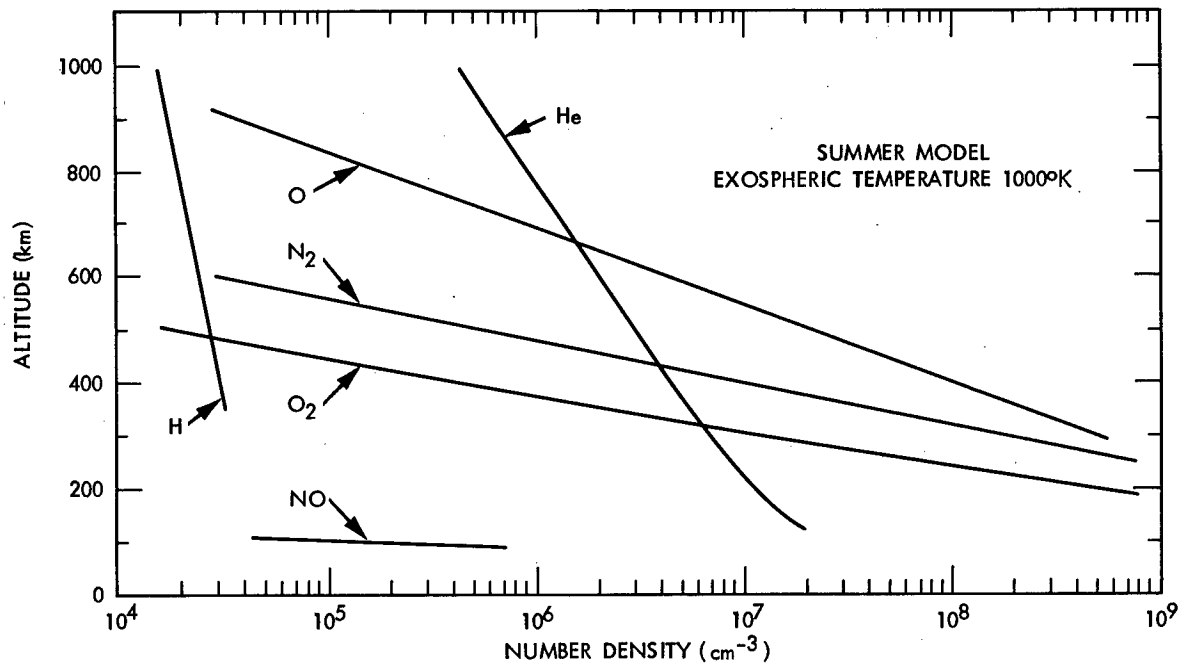

Figure 6 - Neutral atmosphere (ref. 38).

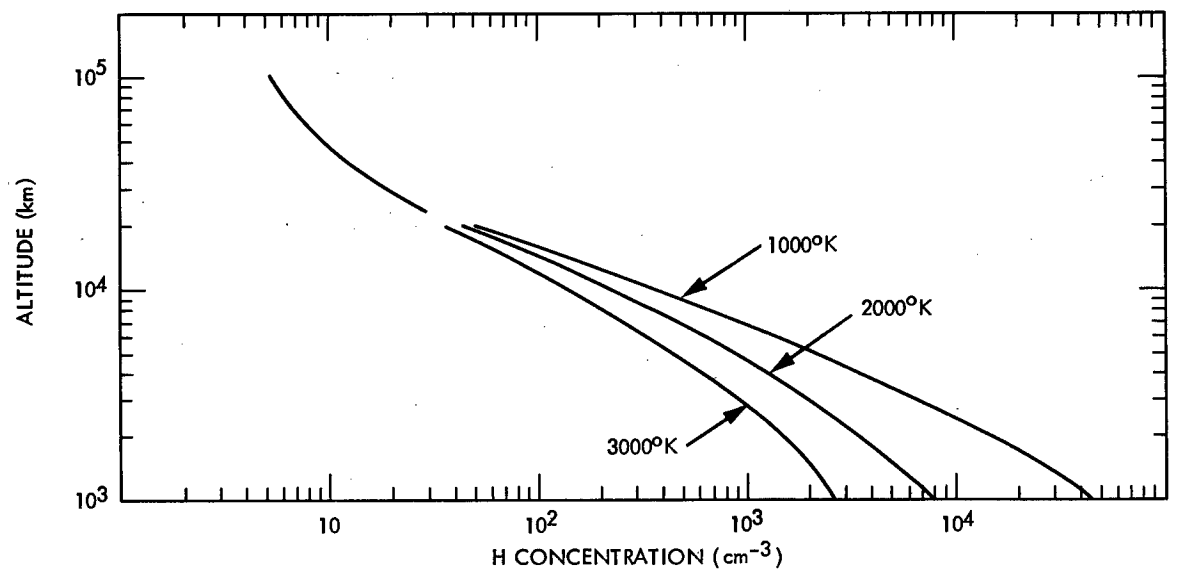

Figure 7 - Neutral atomic hydrogen concentration. Theoretical curves for various H temperatures up to 2×10^4 km; experimental curve for higher altitudes (ref. 38).

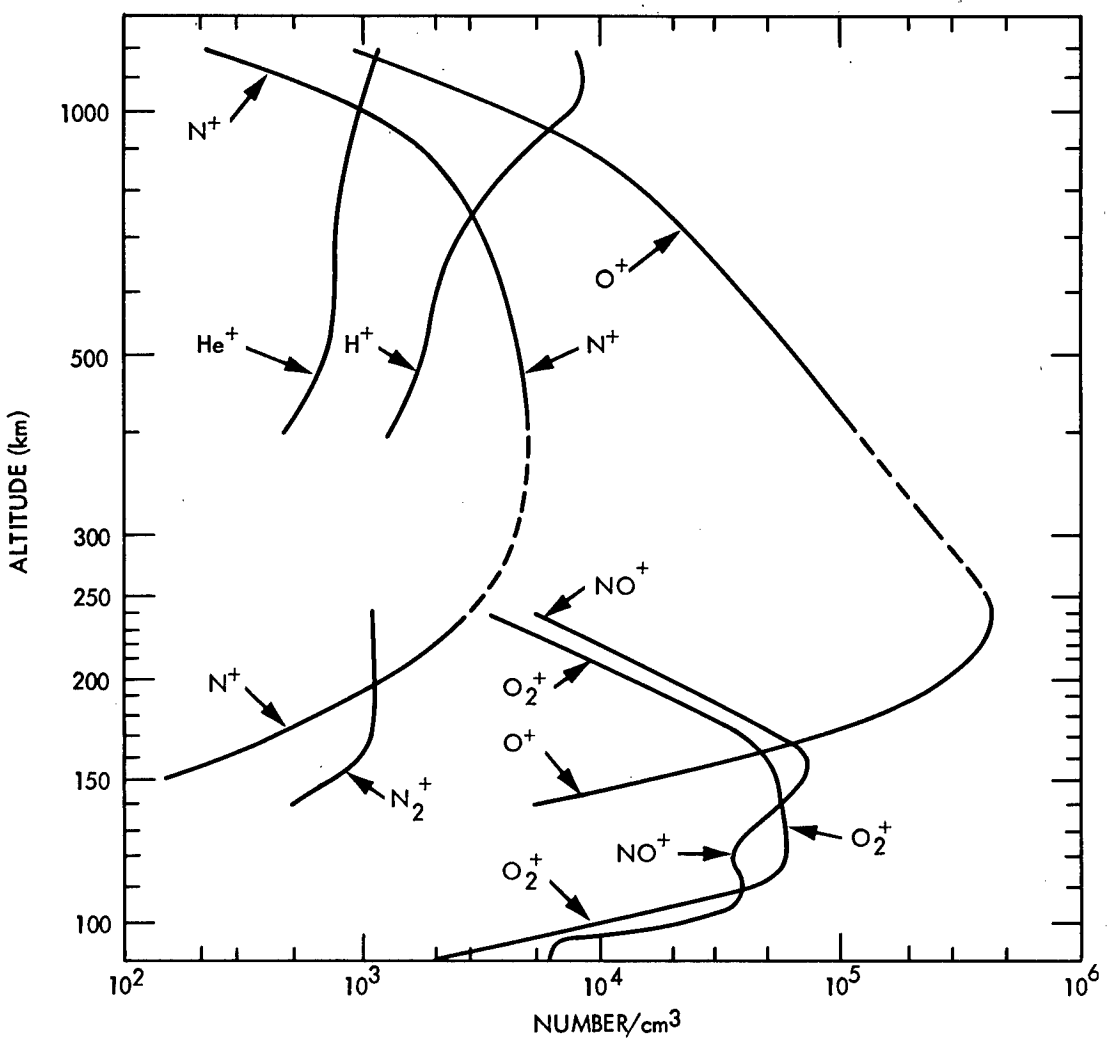

Figure 8 - Ionic composition of solar minimum daytime winter ionosphere (ref. 42).

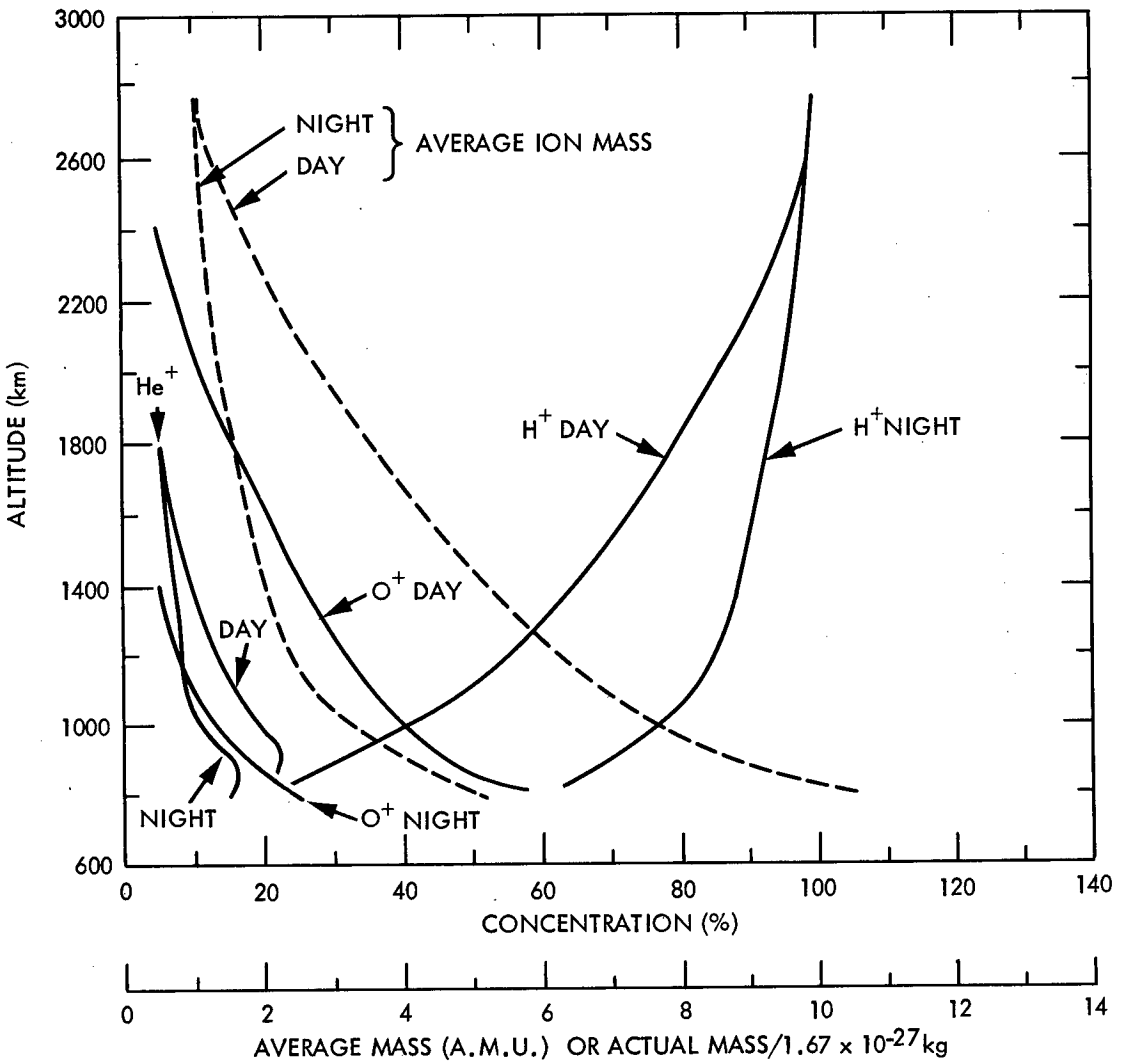

Figure 9 - Relative concentrations of H^+, O^+, and He^+ and their average mass for solar minimum and a quiet summer time. (Nighttime summer profiles are also appropriate for winter daytime.) (ref. 38).

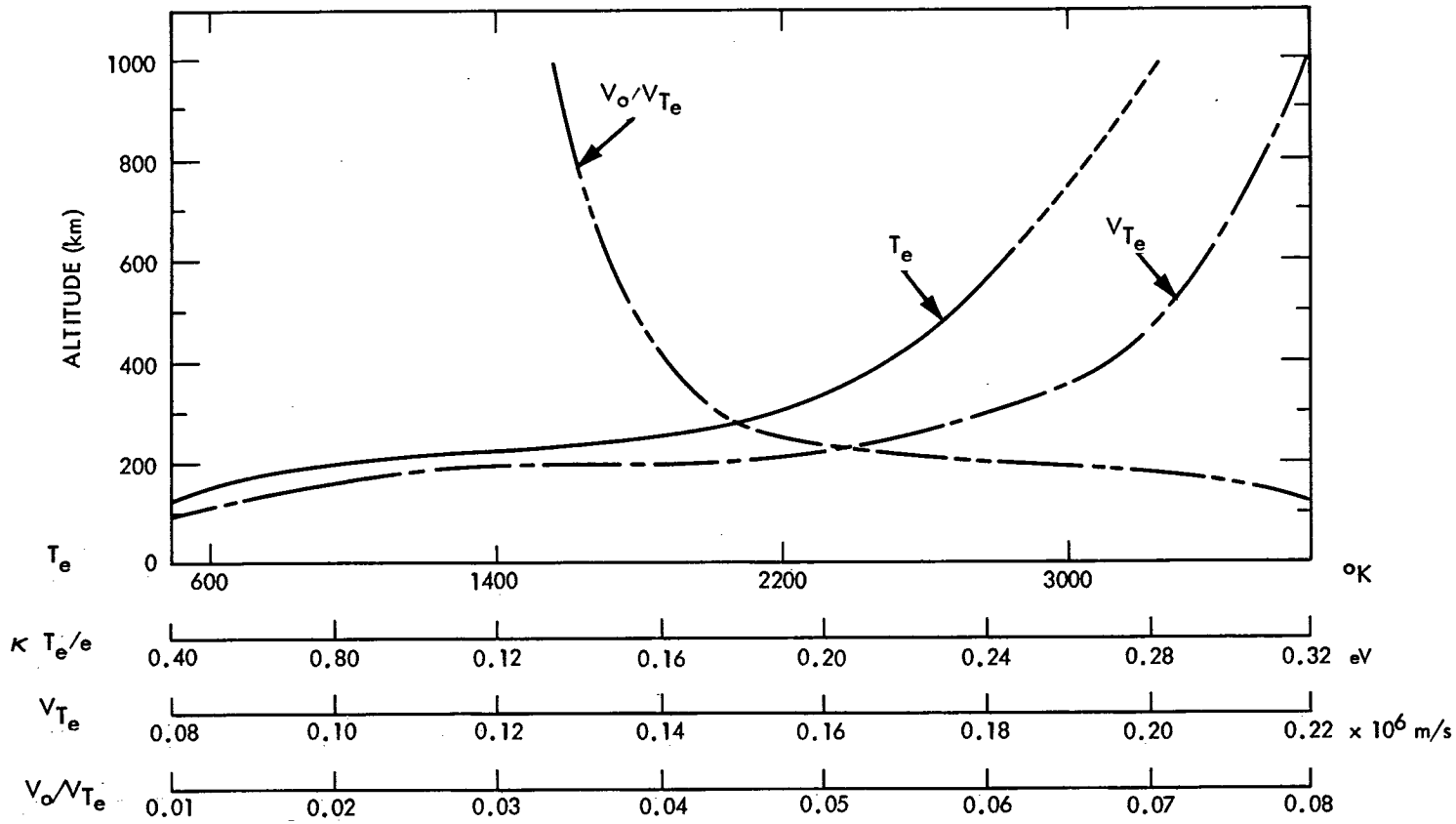

Figure 10 - Electron temperature, thermal velocity, and satellite/thermal velocity ratio (ref. 38).

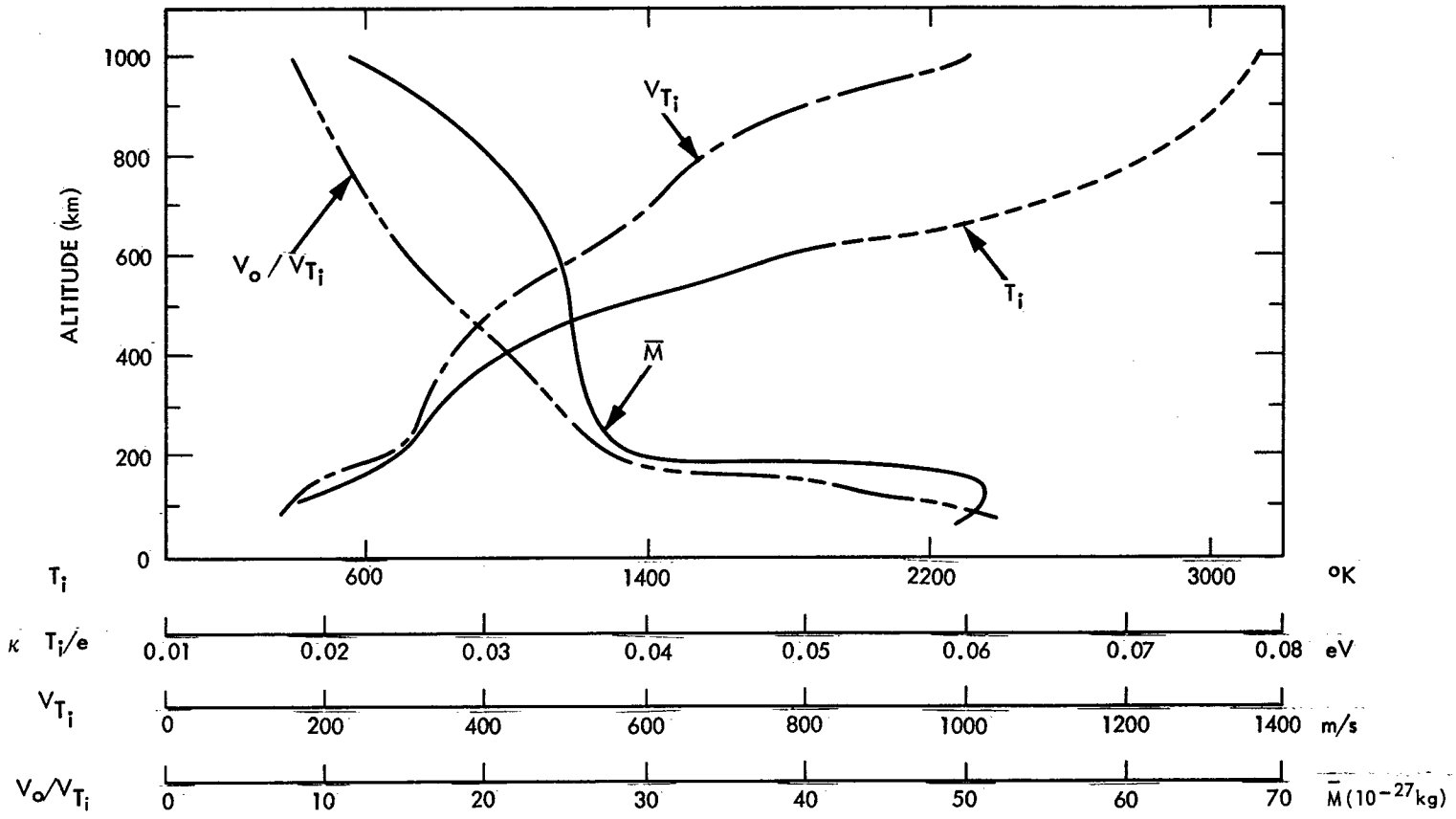

Figure 11 - Ion temperature, thermal velocity, and satellite/thermal velocity ratio (ref. 38).

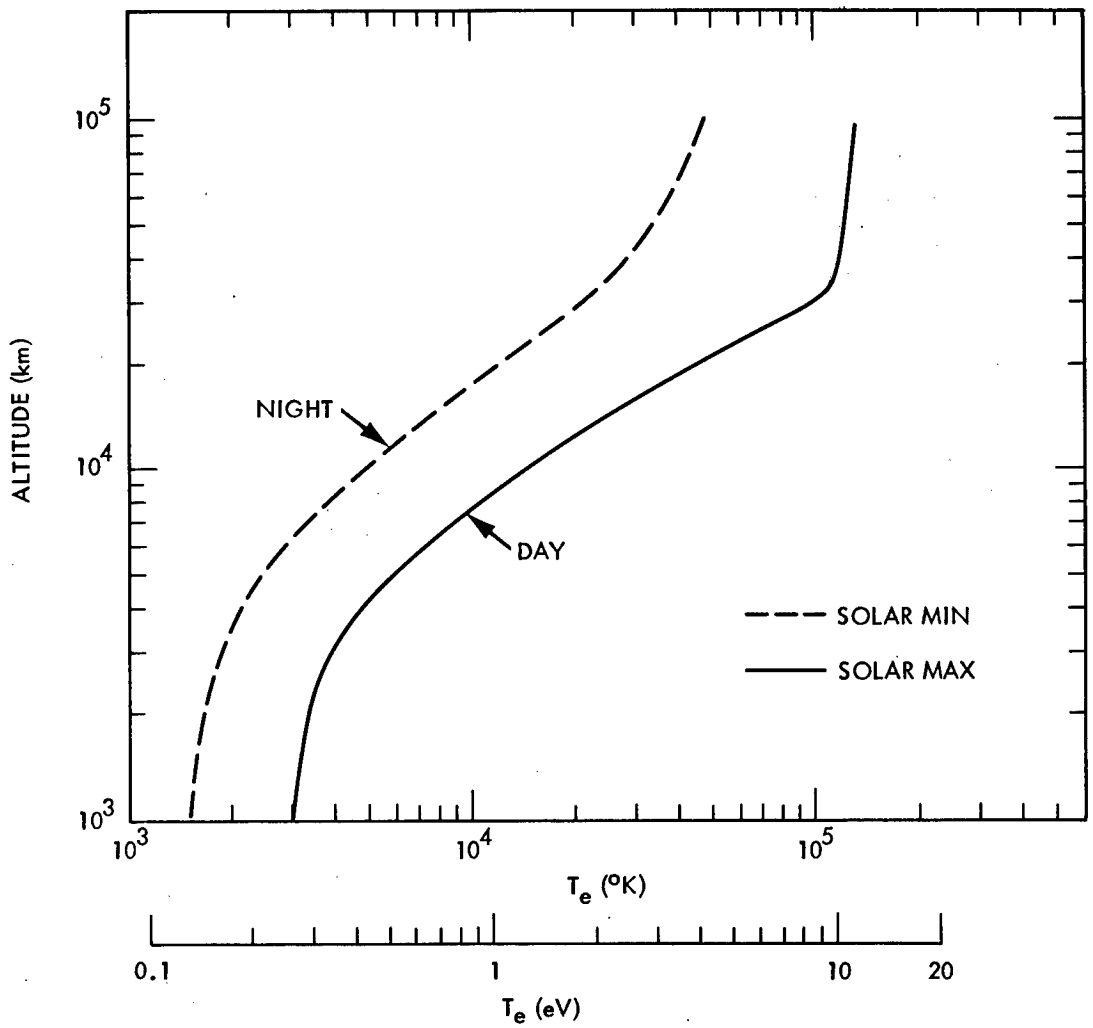

Figure 12 - Models of electron temperature profiles in °K or in eV (viz., $\kappa T_e/e$) (ref. 38).

3.4 Ionospheric Temperature

The electron temperature profiles for daytime summer solar minimum conditions at altitudes below 1000 km are presented in figure 10; the ion temperature profiles are presented in figure 11.

Above 1000 km, the ion temperature is taken as equal to the electron temperature because the ion temperatures theoretically approach the electron temperature values. Figure 12 gives the electron temperature profiles during periods of minimum and maximum solar activity.

3.5 Derived Functions

3.5.1 Thermal Velocities

The thermal velocities of electrons and ions, V_{Te} and V_{Ti}, respectively, the electron temperature, T_e, the average ion mass, $\bar{M}$, and the velocity ratios, V_o/V_{Te} and V_o/V_{Ti}, of the circular orbital spacecraft velocity to the respective thermal velocities are presented in figures 10 and 11 for altitudes below 1000 km.

Figures 13 and 14 give the above functions and the Alfven velocity, V_A, for altitudes above 1000 km.

3.5.2 Plasma Frequency

For the ionosphere below 1000 km the plasma frequency, f_p, is presented in figure 15.

For altitudes above 1000 km, figure 16 gives the plasma frequency, the cyclotron frequency (gyrofrequency) with separate ordinate scales for protons and electrons, F_H and f_H; the lower hybrid frequency, f_{LH}; and the ratio, f_p / f_H. The cyclotron frequency is calculated for a dipole magnetic field in the equatorial plane. Therefore, near the poles and for altitudes above 4 Earth radii, the curves represent only a first order of approximation.

3.5.3 Debye Length

The Debye length, λ_D, is presented in figure 17 for the ionosphere below 1000 km. Also included is the number of particles in a Debye sphere, N_{DS}, where

$$N_{DS} = \frac{4}{3}\pi n_e \lambda_D^3$$

with n_e being the electron concentration. Fluid plasma theory requires that N_{DS} be $>> 1$. Figure 17 shows this condition to exist and actually improve with increasing altitude.

For the ionosphere above 1000 km, the Debye length, λ_D, and the Larmor radii for ions and electrons, R_H and r_H, are presented in figure 18. It should be noted that in the range of altitudes between 2000 and 8000 km the electron Larmor radius becomes comparable to the satellite size ($\sim$ 50 cm). The same occurs for the Debye length at higher altitudes. This can lead to complications in the considerations of the spacecraft interactions with the ionosphere because the selection of the theoretical approach depends on the relative magnitude of the spacecraft dimensions to the Debye length and Larmor radius.

For altitudes below 1000 km, the values of the Larmor radii are presented in figure 19.

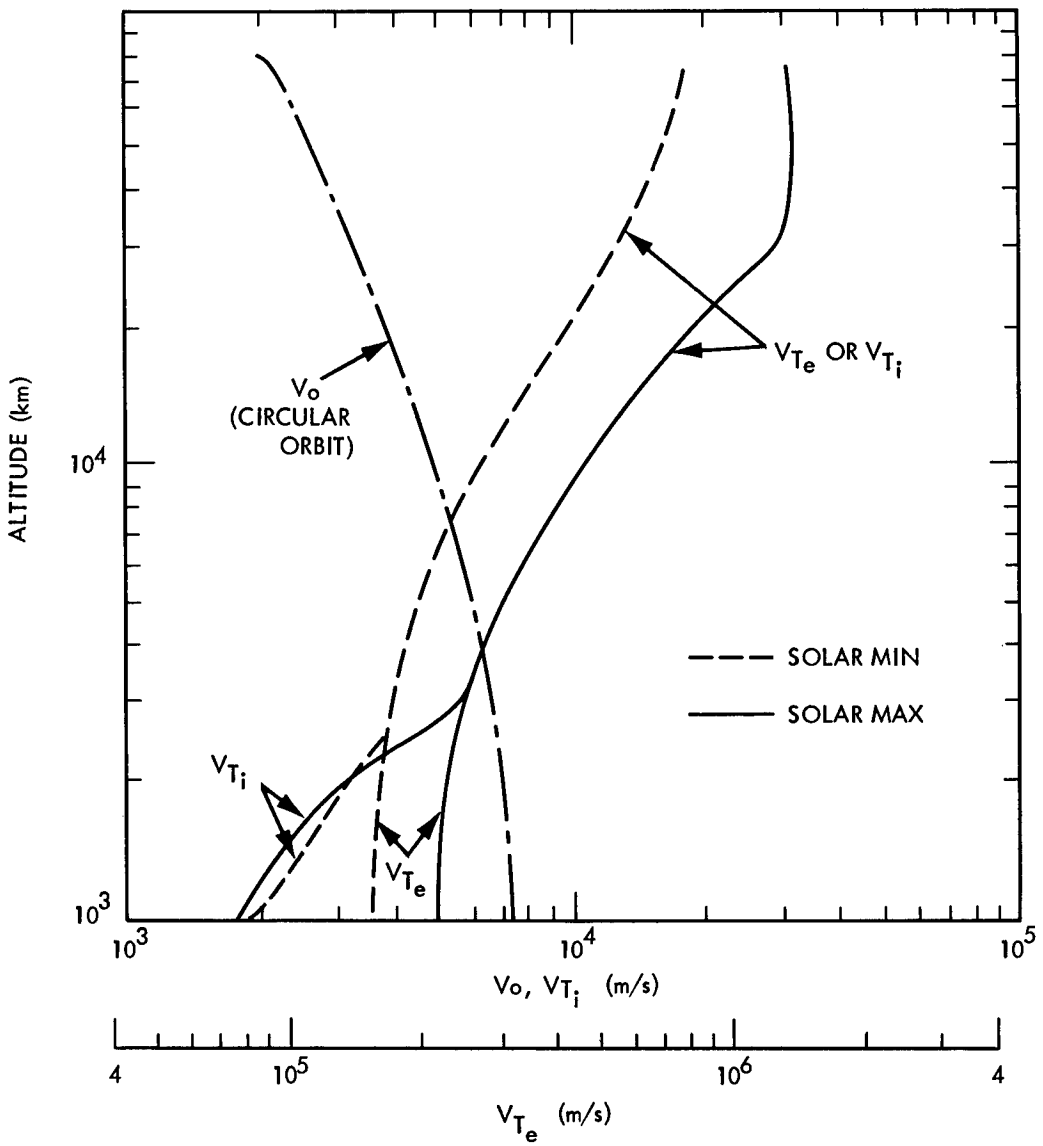

Figure 13 - Satellite velocity V_o, electron thermal velocity V_{T_e}, and ion average velocity V_{T_i} versus altitude above 1000 km (ref. 38).

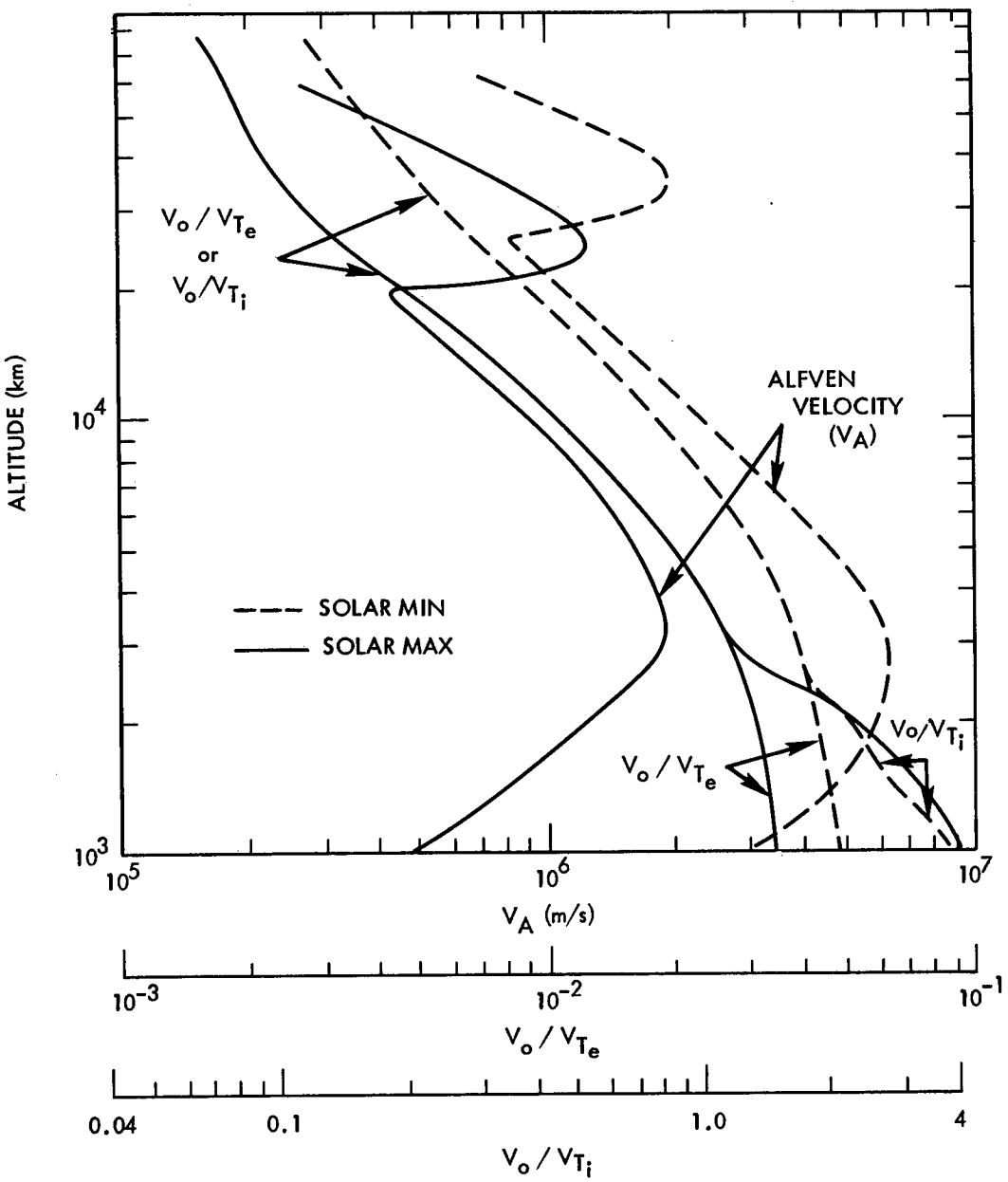

Figure 14 - Alfven velocity V_A, and the ratios V_o/V_{T_e} and V_o/V_{T_i} versus altitude above 1000 km (ref. 38).

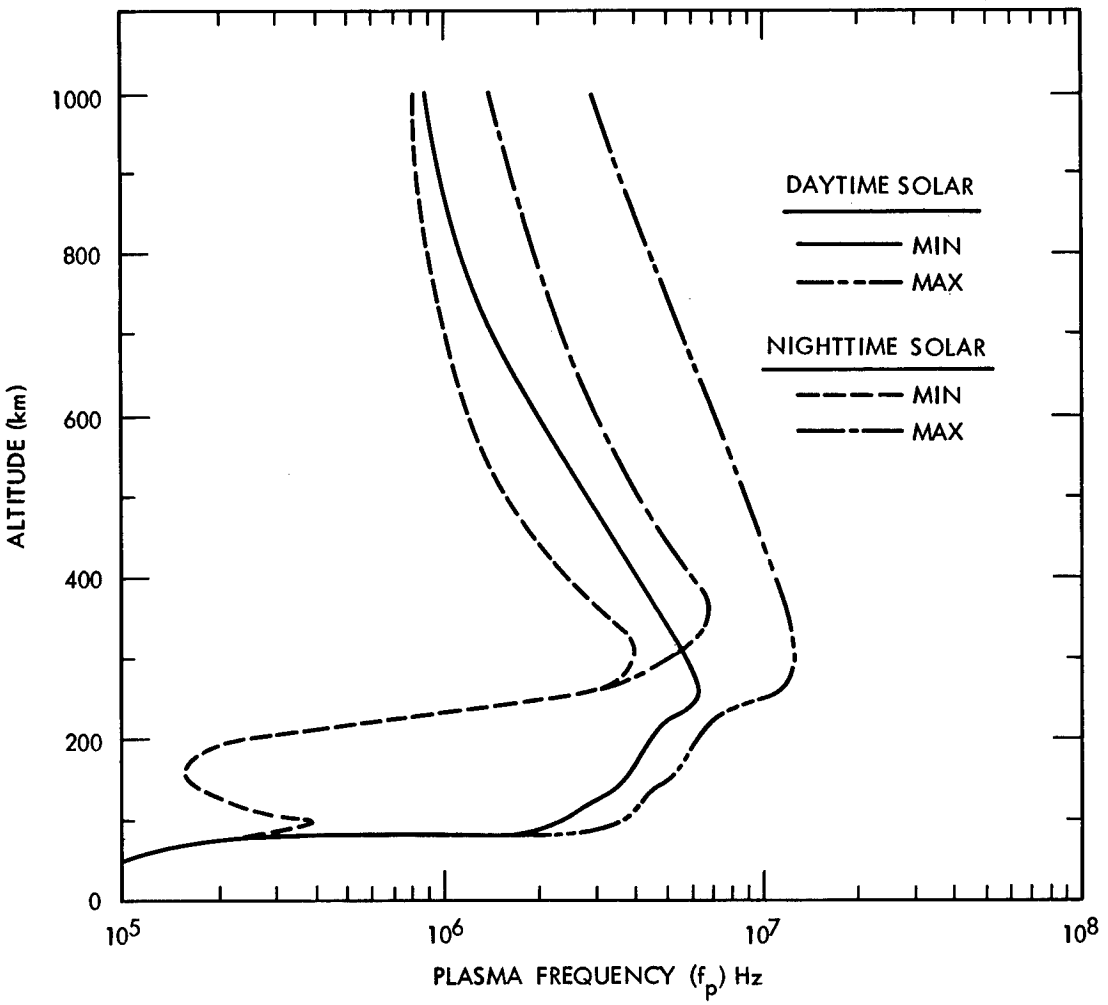

Figure 15 - Electron plasma frequency (ref. 38).

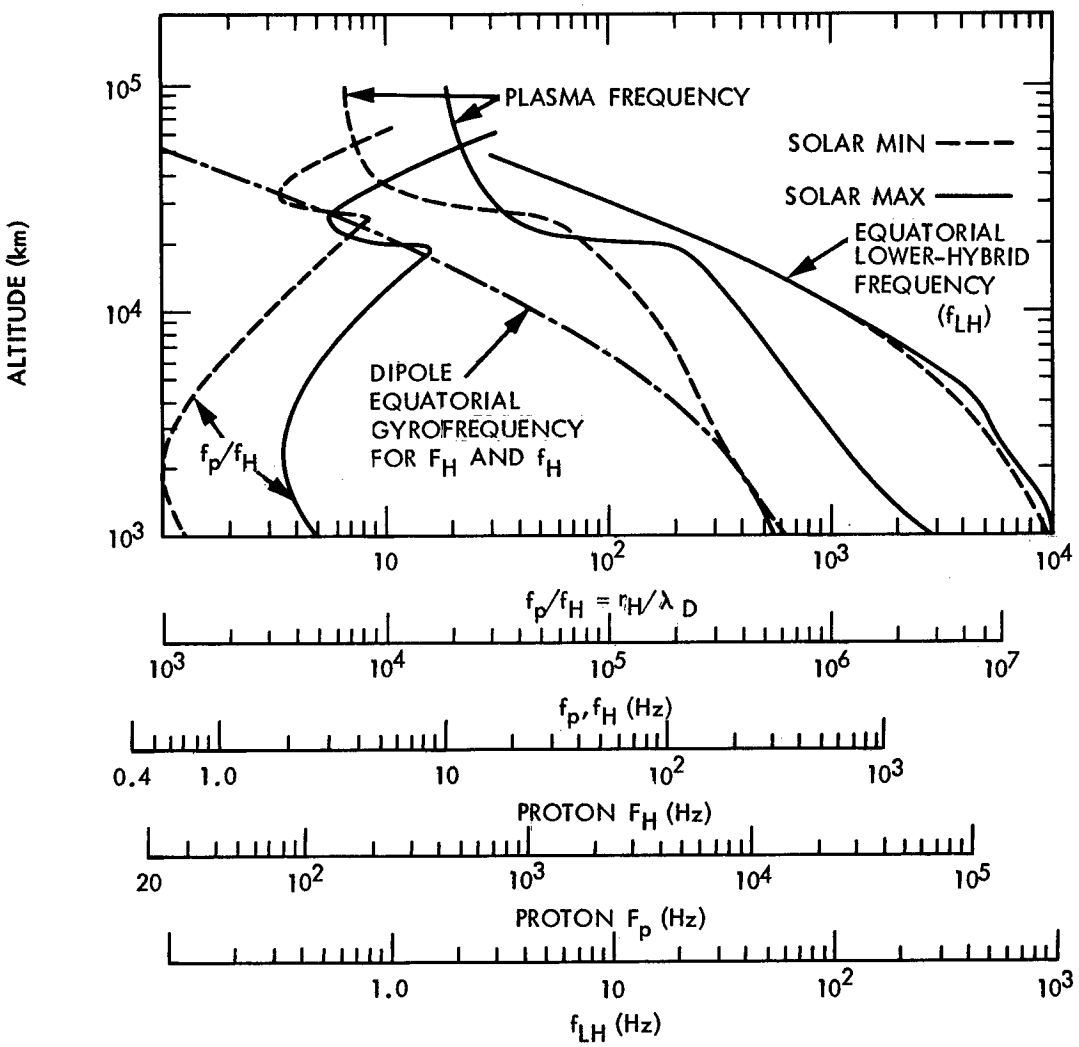

Figure 16 - Electron and proton plasma and cyclotron frequencies (gyrofrequencies) and the ratio f_p/f_H or r_H/λ_D (ref. 38).

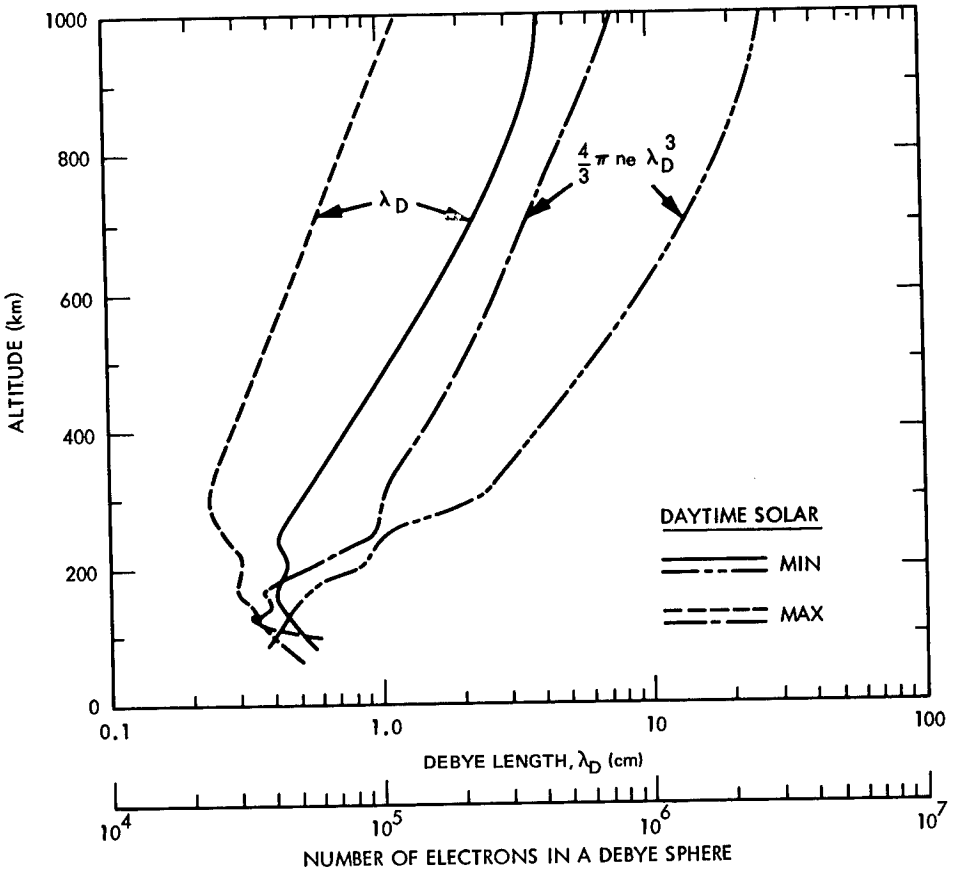

Figure 17 - Debye length (ref. 38).

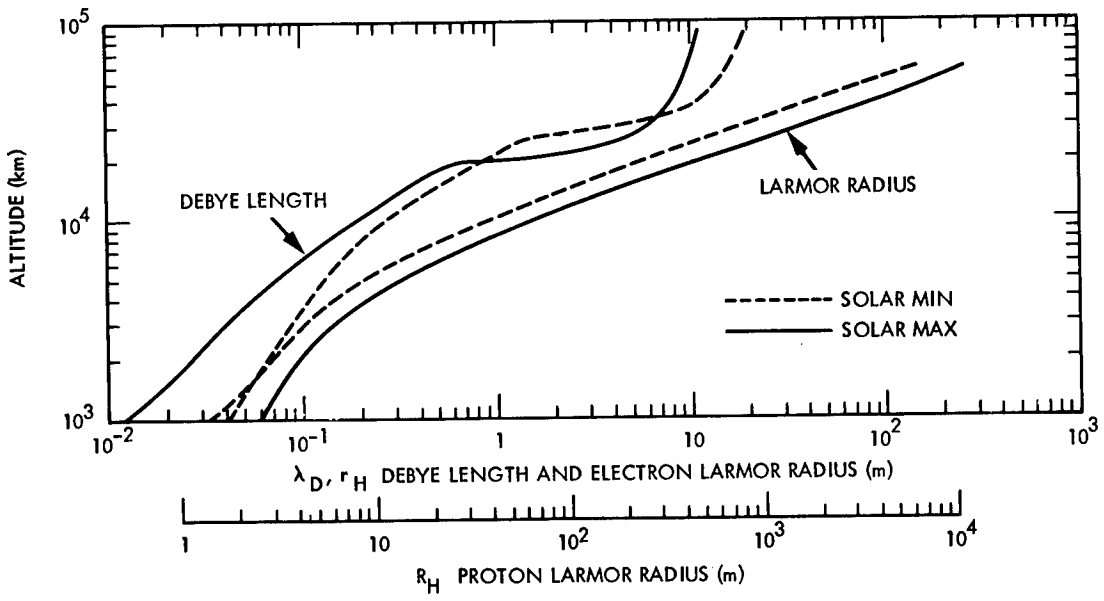

Figure 18 - Debye length and electron and proton Larmor radius (ref. 38).

3.5.4 Collision and Cyclotron Frequencies

The variations of collision frequencies of electrons, ν_e, and the electron mean free path, e_{mfp}, with altitudes below 1000 km are presented in figure 20.

The cyclotron frequencies for electrons, f_H, and ions, F_H, for altitudes below 1000 km are presented in figure 19; for altitudes above 1000 km, the frequencies are presented in figure 16. (The cyclotron frequency must be considered in dealing with a magnetoplasma.)

The angular frequencies of electrons, ω_H, and ions, Ω_H, as well as the Larmor radii for electrons, r_H, and ions, R_H, are also presented in figure 19.

3.5.5 Thermal Particle Flux to a Spacecraft at Plasma Potential

Particle fluxes for electrons and ions at altitudes below 1000 km are presented in figure 21; fluxes above 1000 km, in figure 22. For electrons, the number of particles flowing through unit area is based on the electron thermal velocity, V_{Te}; for ions, the number is based on the satellite orbital velocity, V_o (circular orbit). The orbital velocity is used as a basis for the ion flux because it is generally greater than the ion thermal velocity, V_{Ti}.

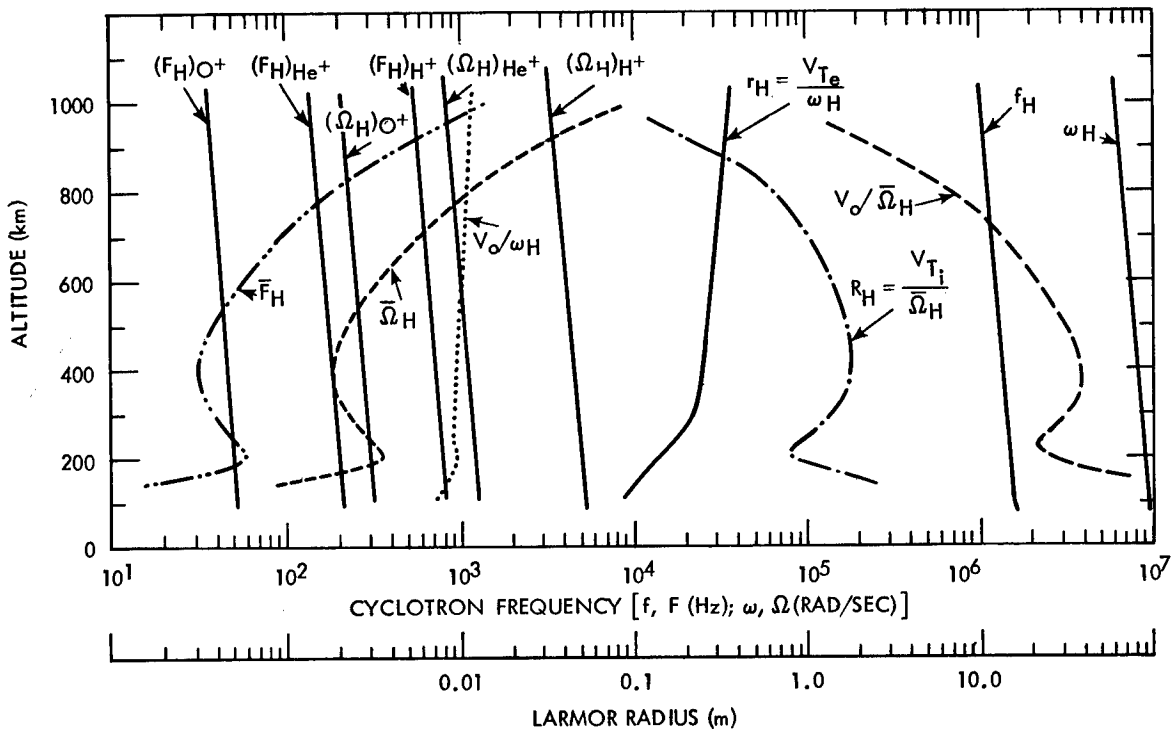

Figure 19 - Cyclotron frequencies and Larmor radii (ref. 38).

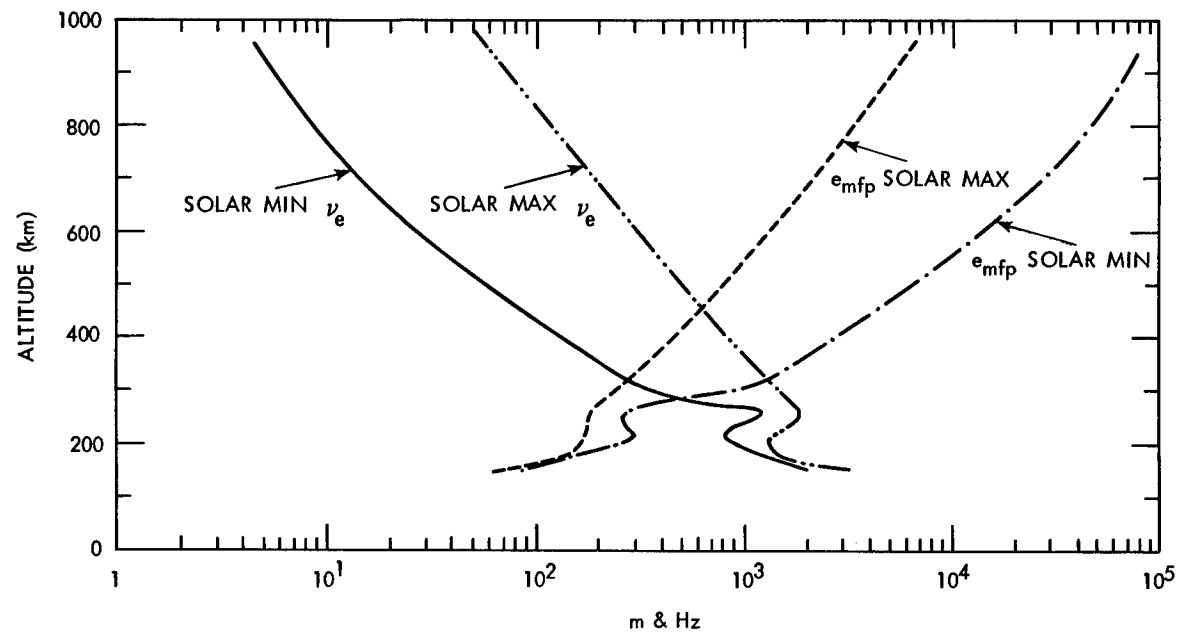

Figure 20 - Electron collision frequencies and mean free paths (ref. 38).

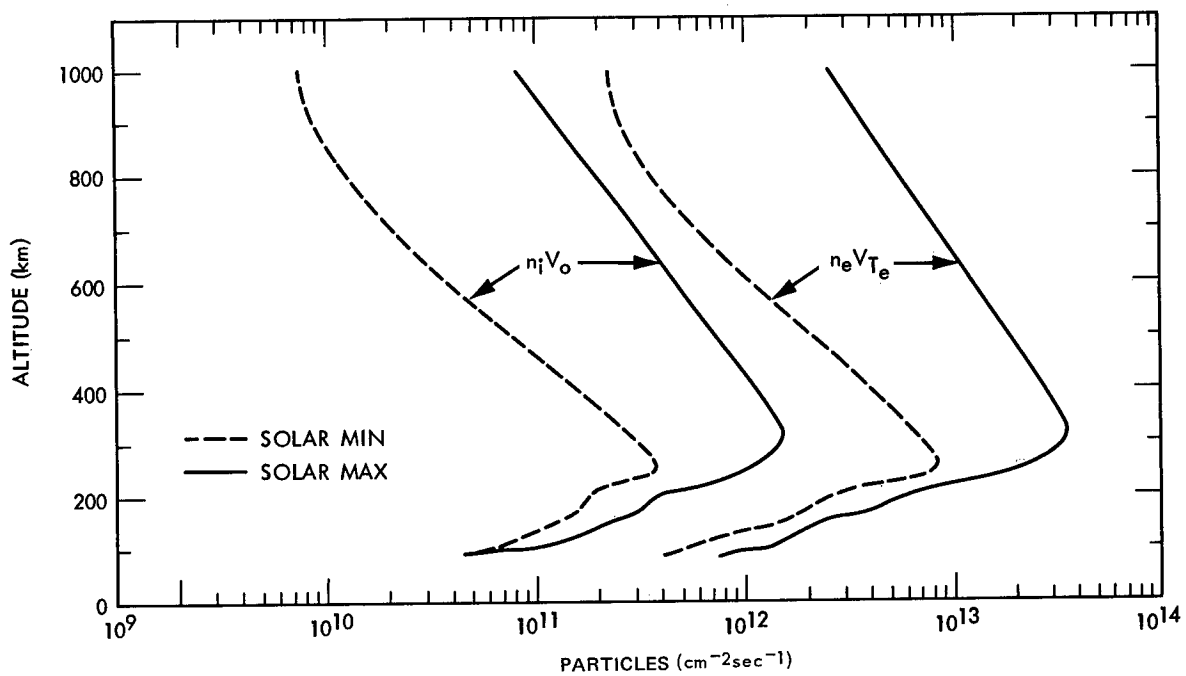

Figure 21 - Thermal particle flux daytime (ref. 38).

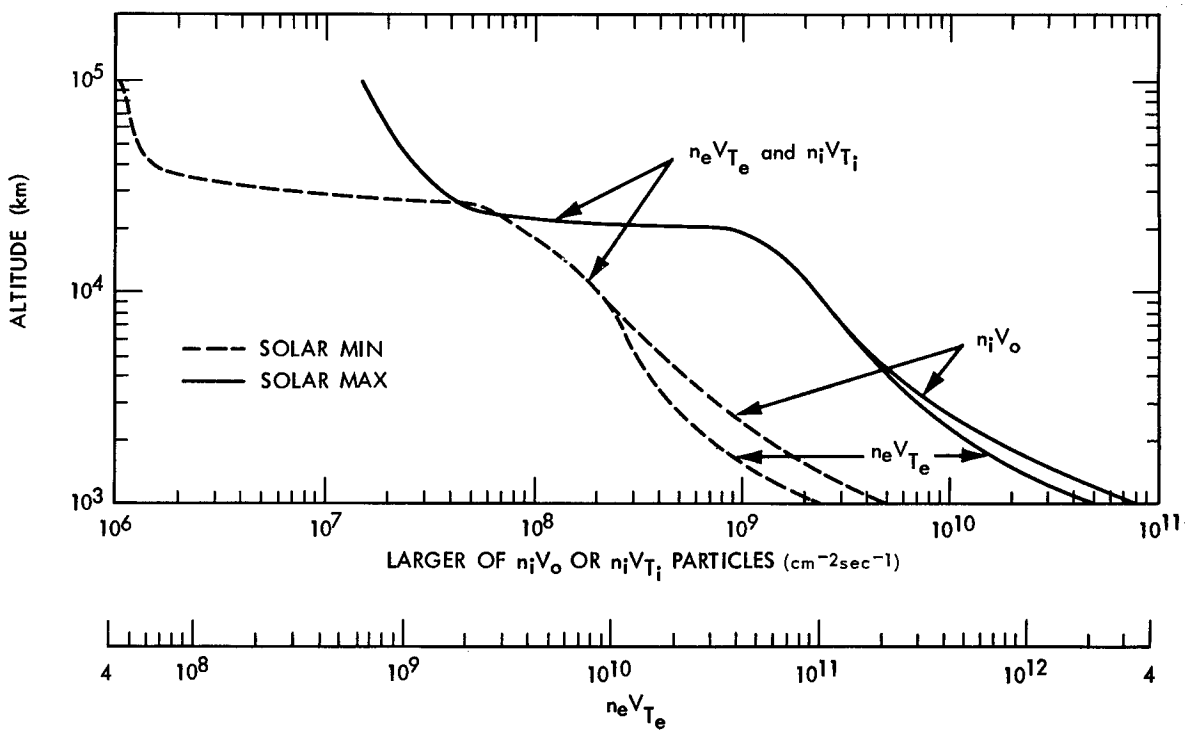

Figure 22 - Thermal electron and ion particle fluxes (ref. 38).

APPENDIX A
Evaluation of the Spacecraft Potential

The general equation for determining the potential on a spherical, electrically conducting spacecraft in circular orbit in the ionosphere is (ref. 38):

$$\phi_o = -\frac{\kappa T_e}{e} \ln \frac{2AB(\kappa T_e/2\pi m_e)^{1/2}}{\left[\left(\frac{8\kappa T_i}{\pi \bar{M}} + V_o^2\right)^{1/2} - \frac{2e\phi_o}{\bar{M}\left(\frac{8\kappa T_i}{\pi \bar{M}} + V_o^2\right)^{1/2}} + \frac{i_{ph}}{n_e}\right]} \qquad (1)$$

where:

ϕ_o = satellite potential (volts)
κ = Boltzmann's constant (joules/°K)
e = Electron charge (coulombs)
T_e = electron temperature (°K)
m_e = electron mass (kg)
T_i = ion temperature (°K)
$\bar{M}$ = average ion mass (kg)
V_o = satellite velocity (m/s)
i_{ph} = photoelectric current (amps/m^2)
n_e = electron density (m^{-3})

The factor AB governs the collection of electrons on the surface of the spacecraft. The factor A varies between 1 and 2 and specifies the amount of electron collection taking place in the spacecraft wake (A=1, no collection; A=2, no wake effect, collection of electrons uniform over the surface). The flow of current to a sensor mounted on the surface of the Explorer 8 spacecraft was investigated (ref. 43) and very little, if any, evidence for an electron wake was found. Laboratory work, reported in reference 44, indicated a lack of electrons in the center of the wake structure, and so it seems reasonable to assume that the wake does have some effect, but the electron collection is only decreased by a small amount, about 5-10%, i.e., A≈1.9. The factor B takes into account the effect of the ambient magnetic field on the electron collection, such that $\frac{1}{2} \leqslant B \leqslant 1$. For B = ½ the magnetic field is considered to be restricting the collection of electrons, and for B=1 the magnetic field is ignored. Equation 1 will be valid only if the spacecraft net charge is negative. This will be true if the argument of the logarithm is $\geqslant 1$. For further discussion and for the case of a positive spacecraft, reference 38 should be consulted.

Equation 1 can be modified to give the spacecraft potential for different ranges of altitude. Thus, after simplification and substitution of appropriate values for constants, the following equations for the spacecraft potential are obtained.

$$\phi_o = (-8.6)10^{-5} T_e \ln \frac{2956\sqrt{T_e}}{V_o} < 200 \text{ Km} \qquad (2)$$

$$= (-8.6)10^{-5} T_e \ln \frac{2956\sqrt{T_e}}{V_o\left(1-\frac{2e\phi_o}{\bar{M}V_o^2}\right)} \quad \text{between 200 and 1000 km}$$

$$= (-8.6)10^{-5} T_e \ln \frac{2956\sqrt{T_e}}{\left[V_o\left(1-\frac{2e\phi_o}{\bar{M}V_o^2}\right)+\frac{i_{ph}}{ne}\right]} \quad \text{between 1000 and 2000 km}$$

$$= (-8.6)10^{-5} T_e \ln \frac{5912\, B\sqrt{T_e}}{\left[\left(\frac{3.5T_i10^{-23}}{\bar{M}}+V_o^2\right)^{1/2}-\frac{2e\phi_o}{\bar{M}\left(\frac{3.5T_i10^{-23}}{\bar{M}}+V_o^2\right)^{1/2}}+\frac{i_{ph}}{ne}\right]}$$

above 2000 km, where B = ½ below 8000 km, B = 1 above 20,000 km, and increases from ½ → 1 linearly between 8,000 and 20,000 km.

APPENDIX B
Waves in the Ionosphere

B.1 Introduction

The basic waves of the cold plasma (one in which each particle species is represented by an "average particle" or fluid model) are the electron, ion, and Alfven waves. Reference 44 analyzes the cold plasma model and presents analytical treatments applicable to certain aspects of electromagnetic waves in plasmas.

Consideration of wave phenomena in the ionosphere covers a range of frequencies from well above 10 MHz to ultra-low frequencies with periods of several seconds.

B.2 High Frequencies

At very high frequencies (including most space telemetry frequencies) well above the higher characteristic frequencies of the ionospheric plasma ($f_p \sim 10$ MHz; $f_H \sim 1$ MHz), the effects are small and can be neglected for operational purposes. These small effects on satellite beacon signals can be used as ionospheric diagnostics, however. They include the Faraday rotation and associated fading rates, the Doppler effect, refraction from density gradients, and scintillation from ionospheric fluctuation (ref. 45, pp. 207-214). An important related parameter is the columnar electron density (electron content, $\int_o^h$ Ndh), which is directly measured by the Faraday and Doppler experiment and has to be considered in the selection of frequencies for tracking systems.

B.3 Medium and Low Frequencies

The frequency range 100 KHz – 20 MHz long has been used to sound or probe the ionosphere with ground-based swept frequency sounders (ref. 45, chapt. 3). More recently satellites systems have been used successfully (refs. 46 through 49) with improved ionogram reduction (ref. 50). The local characteristic frequencies, f_p and f_H, have been inferred directly on ionogram features with good self-consistency (refs. 48 and 51) and otherwise puzzling features fit well into plasma theory (refs. 49 and 52).

B.4 Very-Low Frequency Whistlers (100 Hz - 30 kHz)

Whistlers have been studied extensively for many years from ground stations (refs. 53 and 54) and have yielded much information about the magnetosphere between 2 and 6 earth radii. Satellite observations (refs. 55 and 56) have added a great deal and allowed the observation of ion whistlers and hence local ion composition near the satellite. There are also periodic emissions whose nature is not well understood (ref. 57, chapt. 8, and refs. 53 and 54).

B.5 Ultra-Low Frequencies — Ion and Alfven Waves (10 Hz and Below)

In the vicinity of ion (proton) gyro frequencies at several earth radii and below, the wavelengths and periods are very long and observations and determinations of wave types are more difficult with isolated probes such as satellites. However, much has been done with ground station measurement of magnetic fields (refs. 58, 59 and ref. 57, chapt. 8) and some interesting results have been obtained by satellites (ref. 60). Like the very-low frequency whistlers, the ultra-low frequency range has periodically recurring emissions whose nature is not well understood.

APPENDIX C

Antennas in Plasmas

C.1 Introduction

The preceding discussion on electromagnetic waves in plasmas and specific consideration of the ionospheric plasma provides some understanding of the wave phenomena as they appear in the results of various experiments and also forms a basis for a discussion of the behavior of antennas in plasmas.

The antennas on an orbiting spacecraft are surrounded by plasma which may affect their receiving and radiating properties. The following techniques give quantitative results when the plasma effects are relatively small. Descriptions of work done on more complicated problems may be found in references 61 and 62. The following discussion is restricted to dipole antennas operating at below 100 MHz because, as shown before, at greater frequencies the plasma effects are negligible and at lower frequencies the antennas tend to be arrays of electric or magnetic dipoles. Information on other types of antennas may be found in references 63 through 65.

C.2 Small Dipoles

For elementary dipoles in cold plasmas without a static magnetic field the problem is that of an antenna embedded in an isotropic dielectric, and the impedance may be found from standard antenna texts (e.g., chapt. 2, ref. 66).

For the small single-turn loop (magnetic dipole) it is

$$Z = \frac{\pi(\mu_o/\epsilon_o)^{1/2}\mu_o^{\,2}\omega^4 b^4}{6} + j\omega\mu_o\, b\, \ln\frac{b}{a} = K_e^{\,3/2} R_o + jX_o \qquad (3)$$

and for the electric (Hertzian) dipole the corresponding result is

$$Z = \frac{(\mu_o/\epsilon_o)^{1/2}\mu_o\epsilon_o\omega^2 h^2}{6\pi} - j\frac{\ln\frac{h}{a}}{\pi\epsilon_o\omega h} = K_e^{\,1/2} R_o + \frac{j}{K_e} X_o \qquad (4)$$

where:

μ_o = permeability in free space
ϵ_o = permittivity in free space

In the foregoing expressions, a, b, and h are the conductor radius, loop radius, and diple half length, respectively, and R_o and X_o represent the free space values of resistance and reactance. For a cold isotropic plasma, the dielectric constant is $K_e = 1-\omega_p{}^2/\omega^2$, so the above impedances become

$$Z_{magnetic} = \left(1 - \frac{\omega_p{}^2}{\omega^2}\right)^{3/2} R_o + jX_o \tag{5}$$

$$Z_{electric} = \left(1 - \frac{\omega_p{}^2}{\omega^2}\right)^{1/2} R_o + j \frac{X_o}{1 - \frac{\omega_p{}^2}{\omega^2}} \tag{6}$$

Thus the radiation resistances of both electric and magnetic dipoles decrease as ω decreases to ω_p, but the rate of decrease of the magnetic dipole resistance is greater. Since this magnetic loop is mainly inductive, the loop reactance depends little on the plasma. On the other hand, the Hertzian dipole reactance becomes infinite, implying total reflection or zero power radiation because $\omega \to \omega_p$, in this cold plasma approximation. If the wave frequency is lower than the plasma frequency, the reactance of the electric dipole changes sign. The radiation resistance disappears because no propagating waves are supported by the cold isotropic plasma. Inclusion of temperature corrections associated with plasma waves gives finite corrections at $\omega = \omega_p$ and below for equation 6. In particular, if $\omega_p > \omega \gg \omega_p V_{Te}/c$ and $\omega h/5V_{Te} \gg 1$, the finite residual resistance is $\mu_o V_{Te}{}^2 \omega_p{}^2 h/12 \omega c^2$ where c is velocity of light (ref. 67). The foregoing formula for the reactance of an electric dipole has been used for determining ionospheric electron densities by an RF probe technique (ref. 68).

In actual spacecraft applications the plasmas are anisotropic in the presence of the earth's magnetic field. Infinitesimal dipoles in anisotropic plasmas have been discussed in reference 69 (the infinitesimal loop antenna) and refs. 70 and 71 (the electric dipole).

Analysis of the unrealistic case of a very large static magnetic field for which $\omega_H \gg \omega > \omega_p$ gives relatively simple results. Reference 71 shows that for an infinitesimal electronic dipole aligned parallel to an infinite magnetic field the radiation resistance is

$$R = \frac{60\pi}{\left(\frac{\omega_p}{c}\frac{\omega}{\omega_H}\right)h} \quad \text{for } \omega < \omega_p \tag{7}$$

and

$$R = 20\left(\frac{\omega_p}{c}\frac{\omega}{\omega_H}\right)^2 h^2 \quad \text{for } \omega > \omega_p \tag{8}$$

Equation 8 is similar to the result for an isotropic plasma because the radiation resistance is proportional to the square of the frequency and of the half length (implicit in R_o).

However, the result in equation 7 when $\omega<\omega_p$ is quite different and gives the startling result that the resistance becomes infinite, implying infinite radiation of energy as the dipole length tends to zero.

This peculiarity of the small dipole, which was referred to in reference 72 as the infinity catastrophe, is discussed often in the literature. Some of the problems of the infinity catastrophe can be avoided by assuming non-zero antenna radii (refs. 72 and 73).

Experimental results for the impedance of electric dipole antennas mounted on rockets have been published (refs. 68, 74, 75 and 90). In the experiments the antennas were approximately perpendicular to the earth's magnetic field. In reference 75, some of the experimental data are compared with theoretical impedances obtained from references 73, 76, and 77.

The above comments mainly apply to small dipoles. Research and comments on antennas that are finite but not small compared to a wavelength have been published (refs. 78 through 81).

C.3 Spacecraft Antennas

This section briefly refers to some of the complications that may be encountered by actual spacecraft antennas.

Although temperature effects have not been mentioned, these may be important, especially near various cutoffs and resonances. Wave modes that are absent in cold plasma theory are generated in a non-zero temperature condition and can change the antenna resistance. Finite residual resistance and the importance of temperature below the plasma frequency are discussed in reference 67. Further comments on temperature and antennas can be found in references 82 through 87.

Hitherto, it has been assumed that the plasma medium in which the antenna is embedded is uniform, but in practice this is likely to be unrealistic. The orbit of the vehicle will take it through plasma of varying density. A practical result of this is that the impedance of the antenna and the radiation pattern may change with time so that it is ineffective when operating in some parts of the orbit.

Local inhomogeneity is also likely to be important. Various types of sheath tend to form around satellites and can affect radiation patterns and impedance.

One of the simplest ways to deal with the sheath theoretically is to treat it as a vacuum layer. This is done in references 78, 79, 80, 88, 89, and 90. References 88 and 89 find that the radiation resistance of a sheathed point source in a magnetoplasma is finite for all frequencies. This suggests that inclusion of sheath effects could help to resolve some of the problems associated with the theory of small antennas.

If the RF field of a transmitting antenna is high enough, an RF sheath affecting the antenna's operation may be produced (ref. 91). The RF sheath is associated with radiation involving fairly strong fields. At high signal levels, cross modulation and other non-linear effects may also develop in plasmas surrounding transmitting antennas. It is also possible that in sufficiently strong RF fields breakdown of the surrounding gas will occur. Results on studies of the breakdown of rocket antennas have been reported in reference 90.

References

1. Anon.: Models of Earth's Atmosphere (120 to 1000 km). NASA SP-8021, 1969.

2. Anon.: Magnetic Fields – Earth and Extraterrestrial. NASA SP-8017, 1969.

3. Alpert, Ya. L.: On the Outer Ionosphere and Its Transition into Interplanetary Space. Space Sci. Rev., vol. 6, Feb. 1967, pp. 419-451; Soviet Phys. Uspekhi, vol. 9, no. 6, May-June, 1967, pp. 787-804.

4. Bowles, K. L.: Radio Wave Scattering in the Ionosphere. Measuring Plasma Density of the Magnetosphere. Sci., vol. 139, no. 3553, Feb. 1963, pp. 389-391.

5. Prince, C. E., Jr.; and Bostick, F. X., Jr.: Ionospheric Transmission of Transversely Propagated Plane Waves at Micropulsation Frequencies and Theoretical Power Spectrums. J. Geophys. Res., vol. 69, no. 15, Aug. 1964, pp. 3213-3234, Appendix 2.

6. Carpenter, D. L.: Whistler Studies of the Plasmapause in the Magnetosphere – 1. J. Geophys. Res., vol. 71, no. 3, Feb. 1966, pp. 693-709.

7. Angerami, J. J.; and Carpenter, D. L.: Whistler Studies of the Plasmapause in the Magnetosphere – 2. J. Geophys. Res., vol. 71, no. 3, Feb. 1966, pp. 711-725.

8. Dowden, R. L.; and Emery, M. W.: The Use of Micropulsation Whistlers in the Study of the Outer Magnetosphere. Planetary and Space Sci., vol. 13, no. 8, Aug. 1965, pp. 773-779.

9. Binsack, J. H.: Plasmapause Observations with the M.I.T. Experiment on IMP 2. J. Geophys. Res., vol. 72, no. 21, Nov. 1967, pp. 5231-5237.

10. Brice, N. M., "Bulk Motion of the Magnetosphere", J. Geophys. Res., Vol. 72, No. 21, November 1967, pp. 5193-5211.

11. Anon.: U. S. Standard Atmosphere Supplements, 1966, ESSA, NASA, USAF, Washington, D. C., 1966.

12. Liwshitz, M.: The Effect of Thermal Escape on the Neutral Hydrogen above 120 Kilometers. J. Geophys. Res., vol. 72, no. 1, Jan. 1967, pp. 285-293.

13. Johnson, F. S.; and Fish, R. A.: The Telluric Hydrogen Corona. Astrophysical J., vol. 131, 1960, pp. 502-515.

14. Hoffman, J. H.: A Mass Spectrometric Determination of the Composition of the Nighttime Topside Ionosphere. J. Geophys. Res., vol. 72, 1967, pp. 1883.

15. Barrington, R. E.; and McEwen, D. J.: Ion Composition from VLF Phenomena Observed by Alouette I and II. In Space Research, vol. 2. North-Holland Pubs. Co., Amsterdam, 1967.

16. Bauer, S.J.: Ionizing Radiations and the Constitution of the Upper Atmosphere. In Electron Density Profiles in Ionosphere and Exosphere, edited by J. Frihagen, 1966. (Available from North-Holland Publ Co., Amsterdam)

17. Taylor, H. A.; Brinton, H. C.; and Smith, C. R.: Positive Ion Composition in the Magnetoionosphere Obtained from the OGO-A Satellite. J. Geophys. Res., Vol. 70, no. 23, Dec. 1965, pp. 5769-5781.

18. Gurnett, D. A.; Shawhan, S. D.; Brice, N. M.; and Smith, R. L.: Ion Cyclotron Whistlers. J. Geophys. Res., vol. 70, no. 7, Apr. 1965, pp. 1665-1687.

19. Shawhan, S. D.; and Gurnett, D. A.: Fractional Concentration of Hydrogen Ions in the Ionosphere from VLF Proton Whistler Measurement. J. Geophys. Res., vol. 71, no. 1, Jan. 1966, pp. 47-59.

20. Carlson, H. C.; and Gordon, W. E.: Radar Spectrographic Estimates of Ionic Composition from 225 to 1400 Kilometers for Solar Minimum Winter and Summer Conditions. J. Geophys. Res., vol. 71, no. 23, Dec. 1966, pp. 5573-5578.

21. Johnson, F. S.: Satellite Environment Handbook, 2nd Ed. Stanford University Press, Calif., 1965.

22. Aikin, A. C.; and Bauer, S. J.: The Ionosphere. In Introduction to Space Sciences, 2nd ed., Gordon & Breach Pub., New York, 1968.

23. Evans, J. V.: Midlatitude Electron and Ion Temperatures at Sunspot Minimum. Planet. Space Sci., vol. 15, 1967, pp. 1557.

24. Serbu, G. P.; and Maier, E. J. R.: Low-Energy Electrons Measured on IMP 2. J. Geophys. Res., vol. 71, no. 15, Aug. 1966, pp. 3755-3766.

25. Banks, P. M.: Thermal Conduction and Ion Temperatures in the Ionosphere. Earth and Planetary Sci. Letters, vol. 1, 1966, pp. 270-275.

26. Brace, L. H.; Reddy, B. M.; and Mayer, H. G.: Global Behavior of the Ionosphere at 1000 km Altitude. J. Geophys. Res., vol. 72, 1967, pp. 265-283.

27. Brace, L. H.; Mayer, H. G.; and Reddy, B. M.: The Early Effects of Increasing Solar Activity upon the Temperature and Density of the 1000 Km Ionosphere. J. Geophys. Res., vol. 73, 1968, pp. 1607-1615.

28. Johnson, C. Y.; and Meadows, K. B.: First Investigation of Ambient Positive-Ion Composition to 219 Km by Rocket Borne Spectrometer. J. Geophys. Res., vol. 60, 1955, pp. 193-203.

29. Beard, B. D.; and Johnson, F. S.: Charge and Magnetic Field Interaction with Satellites. J. Geophys. Res., vol. 65, 1960, p. 1.

30. Drell, S. D.; Foley, H. M.; and Ruderman, M. A.: Drag and Propulsion of Large Satellites in the Ionosphere; An Alfven Propulsion Engine in Space. J. Geophys. Res., vol. 70, 1965, pp. 3131.

31. Chu, C. K.; and Gross, R. A.: Alfven Waves and Induction Drag on Long Cylindrical Satellites. AIAA J., vol. 4, 1966, pp. 2209.

32. Hohl, F.: The Electromagnetic Torques on Spherical Earth Satellites in a Rarefied Partially Ionized Atmosphere. NASA Technical Report TR R-231, 1966.

33. Moore, R. D.: Propulsion by the Geomagnetic Field. Space/Aeronautics, vol. 42, 1967, pp. 96.

34. Dickinson, P. H. G.: Positive Ion Sheaths due to V x B. Internal Memo 123, 1964, Dept. Sci. & Ind. Res. U. K.

35. Parker, L. W.: A Computer Program for Calculating the Charge Distribution about a Space Vehicle. NASA CR-401, 1966.

36. Taylor, J. C.: Disturbance of a Rarefied Plasma by a Supersonic Body on the Basis of the Poisson-Vlasov Equations I. Planet. & Space Sci., vol. 15, 1967, pp. 155-187.

37. Kiel, R. E.; Gustafson, W. A.; and Gey, F. C.: Electrostatic Potential Fields of an Ionospheric Satellite. AIAA J., vol. 6, 1968, pp. 708.

38. Kasha, M. A.: The Ionosphere and Its Interaction with Satellites. Gordon and Breach, Science Publishers, New York, 1967.

39. Valley, S. L.: Handbook of Geophysics and Space Environments. McGraw-Hill Book Co., Inc., 1965.

40. Chan, K. L.; and Colin, L.: Global Electron Density Distribution from Topside Soundings. Proceedings of IEEE, vol. 57, no. 6, June 1969, pp. 990-1004.

41. Frihagen, J. (Ed.): Electron Density Profiles in Ionosphere and Exosphere. North-Holland Pubs. Co., Amsterdam, 1966.

42. Johnson, C. Y.: Ionospheric Composition and Density from 90-1200 km at Solar Minimum. J. Geophys. Res., vol. 71, 1966, pp. 330.

43. Bourdeau, R. E.; Donley, J. L.; Serbu, G. P.; and Whipple, Jr. S. C.: Measurements of Sheath Currents and Equilibrium Potential on the Explorer VIII Satellite. J. Astron. Sci., vol. 8, 1961, pp. 65-73.

44. Kasha, M. A.; and Johnston, T. W.: Laboratory Simulation of a Satellite-Mounted Plasma Diagnostic Experiment. J. Geophys. Res., vol. 72, 1967, pp. 4028-4030.

45. Davies, Kenneth: Ionospheric Radio Propagation. U. S. Department of Commerce, National Bureau of Standards Monograph 80, 1965.

46. Nelms, G. L.; Barrington, R. E.; Belrose, J. S.; Hartz, T. R.; MacDiarmid, I. B.; and Brace, L. H.: The Alouette II Satellite. Can. J. Phys. vol. 44, no. 7, July 1966, pp. 1419-1430.

47. Calvert, W.; Van Zandt, T. E.: Fixed Frequency Observations of the Plasma Resonances in the Topside Ionosphere. J. Geophys. Res., vol. 71, no. 7, April 1966, pp. 1799-1813.

48. Calvert, W.; and Goe, G. B.: Plasma Resonances in the Upper Ionosphere. J. Geophys. Res., vol. 68, no. 22, Nov. 1963, pp. 6113-6120.

49. Muldrew, D. B.: Medium Frequency Conjugate Echoes Observed in Topside Sounder Data. Can. J. Phys., vol. 45, no. 12, Dec. 1967, pp. 3935-3944.

50. Jackson, J. E.: The Reduction of Topside Ionograms to Electron Density Profiles, Proceedings of the IEEE, June 1969, pp. 960.

51. Stix, T. H.: The Theory of Plasma Waves. McGraw-Hill, 1962.

52. Calvert, W.: Oblique Z-Mode Echoes in the Topside Ionosphere. J Geophys. Res., vol. 21, no. 23, Dec. 1966, pp. 5579-5583.

53. Helliwell, R. A.: Whistlers and Related Ionospheric Phenomena. Stanford University Press, 1965.

54. Gendrin, R.: Progres Recents dans l'Etude des Ondes TBF et EBF. Space Sci. Rev., vol. 7, pp. 314-395.

55. Gurnett, D. A.; Shawhan, S. D.; Brice, N. M.; and Smith, R. L.: Ion Cyclotron Whistlers. J. Geophys. Res., vol. 70, no. 7, Apr. 1965, pp. 1665-1687.
also
Smith, R. L.; and Brice, N. M.: Propagation in Multicomponent Plasmas. J. Geophys. Res., vol. 69, no. 23, Dec. 1964, pp. 5029-5040.

56. Brice, N. M.: Ion Effects Observed in Radio Wave Propagation in the Ionosphere, and Electromagnetic Wave Theory, Part 1. Proc. Delft. Symp. Sept. 1965, Pergamon, 1967.

57. Hines, C. O.; Paghis, I; Hartz, T. R.; and Fejer, J. A., Ed.: Physics of the Earth's Upper Atmosphere. Prentice-Hall, 1965.

58. Troitskaya, V. A.; Gul'elmi, A. V.: Geomagnetic Micropulsations and Diagnostics of the Magnetosphere. Space Sci. Rev., vol. 7, no. 516, Dec. 1967, pp. 689-768.

59. Hulquist, B: Plasma Waves in the Frequency Range 0.001-10cps in the Earth's Magnetosphere and Ionosphere. Space Sci. Rev., vol. 5, no. 5, Aug. 1966, pp. 599-695.

60. Patel, V. L.: Low-Frequency Hydromagnetic Waves in the Magnetosphere. Explorer XII Planet. Space Sci., vol. 13, no. 6, June 1965, pp. 485-506.

61. Bachynski, M. P.: Sources in Plasmas. RCA Review, vol. 28, 1967, pp. 111.

62. Walsh, P.; and Haddock, F. T.: Antenna Impedance in a Plasma: Problems Relevant to Radio Astronomy Measurements from Space Vehicles. Annales d'Astrophysique, vol. 28, 1965, pp. 605.

63. Galejs, J.; and Mentzoni, M. H.: Waveguide Admittance for Radiation into Plasma Layers – Theory and Experiment. IEEE Trans. Antennas Propagation, vol. AP-15, 1967, pp. 465.

64. Owyang, G. H.; and Seshadri, S. R.: Radiation Conductance of a Slot Covered with Anisotropic Plasma. Proc. Instn. Elect. Engrs. (G.B.), vol. 113, 1966, pp. 1920.

65. Waletsko, J. A.; and Bekefi, G.: RF Admittance Measurements of a Slotted-Sphere Antenna Immersed in a Plasma. Radio Sci., vol. 2, 1967, pp. 489.

66. King, R. W. P.: The Theory of Linear Antennas. Harvard University Press, Cambridge, Mass., 1956.

67. Kuehl, H. H.: Computations of the Resistance of a Short Antenna in a Warm Plasma. Radio Sci., vol. 2, 1967, pp. 73.

68. Jackson, J. E.; and Kane, J. A.: Measurements of Ionospheric Electron Densities Using an RF Probe Technique. J. Geophys. Res., vol. 64, 1959, pp. 1074.

69. Weil, H.; and Walsh, D.: Radiation Resistance of an Elementary Loop Antenna in a Magnetoionic Medium. IEEE Trans. Ant. and Prop., vol. AP-13, 1965, pp. 21.

70. Kuehl, H. H.: Electromagnetic Radiation from an Electric Dipole in a Cold Anisotropic Plasma. Phys. Fluids, vol. 5, 1962, pp. 1095.

71. Seshadri, S. R.: Radiation Resistance of a Linear Current Filament in a Simple Anisotropic Medium. IEEE Trans. Ant. and Prop., vol. AP-13, 1965, pp. 819.

72. Staras, H.: The Impedance of an Electric Dipole in a Magneto-Ionic Medium. IEEE Trans. Ant. and Prop., vol. AP-12, 1964, pp. 695.

73. Balmain, K. G.: The Impedance of a Short Dipole Antenna in a Magnetoplasma. IEEE Trans. Ant. and Prop., vol. AP-12, 1964, pp. 605.

74. Stone, R. G.; Weber, R. R.; and Alexander, J. K.: Measurement of Antenna Impedance in the Ionosphere – I: Observing Frequency Below the Electron Gyro Frequency. Planet. and Space Sci., vol. 14, 1966, pp. 631.

75. Stone, R. G.; Alexander, J. K.; and Weber, R. R.: Measurements of Antenna Impedance in the Ionosphere – II: Observing Frequency Greater than the Electron Gyro Frequency. Planet. Space Sci., vol. 14, 1966, pp. 1007.

76. Ament, W. S.; Datzin, M.; McLaughlin, J. R.; and Zachary, W. W.: Electromagnetic Research Corp. Report no. NAS 5835-1. College Park, Md., 1964.

77. Herman, J. R.: The Impedance of a Rocket-Borne Capacitive Ionospheric Probe. J. Geophys. Res., vol. 69, 1964, pp. 3299.

78. Galejs, J.: Impedance of a Finite Insulated Cylindrical Antenna in a Cold Plasma with a Longitudinal Magnetic Field. IEEE Trans. Ant. and Prop., vol. AP-14, 1966, pp. 727.

79. Galejs, J.: Impedance of a Finite Insulated Antenna in a Cold Plasma with a Perpendicular Magnetic Field. IEEE Trans. Ant. and Prop., vol. AP-14, 1966, pp. 737.

80. Galejs, J.: Variationally Computed Antenna Impedances and Accuracy of Resulting Current Distributions. Electronics Letters, vol. 3, 1967, pp. 371.

81. Cook, K. R.; and Johnson, G. L.: On the Problem of the Infinite Antenna in an Anisotropic Plasma. Radio Sci., vol. 2, 1967, pp. 495.

82. Whale, H. A.: The Excitation of Electroacoustic Waves by Antennas in the Ionosphere. J. Geophys. Res., vol. 68, 1963, pp. 415.

83. Carlin, J.; and Mittra, R.: Effects of Induced Acoustics Sources on the Impedance of a Cylindrical Dipole in a Warm Plasma. Radio Sci., vol. 2, 1967, pp. 1327.

84. Kuehl, H. H.: Excitation of a Warm Plasma by an Electric Dipole. J. Math. Phys., vol. 45, 1966, pp. 318.

85. Shkarofsky, I. P.; Johnston, T. W.; and Bachynski, M. P.: The Particle Kinetics of Plasmas. Addison-Wesley Publ. Co., Reading, Mass., 1966.

86. Chen, K. M.; Judson, H.; and Liu, C. C.: Experimental Study of an Electroacoustic Wave excited by an Antenna in a Hot Plasma. Proc. IEEE, vol. 55, 1967, pp. 1656.

87. Wunsch, A. D.: Current Distribution on a Dipole Antenna in a Warm Plasma. Electronics Letters, vol. 3, 1967, pp. 320.

88. Seshadri, S. R.; and Bhatnagar, K. L.: Effect of Ion Sheath on Radiation in a Magnetoionic Medium – I: Source Current Parallel to the Magnetostatic Field. Can. J. Phys., vol. 44, 1966, pp. 1401.

89. Seshadri, S. R.; and Bhatnagar, K. L.: Effect of Ion Sheath on Radiation in a Magnetoionic Medium – II: Source Current Perpendicular to the Magnetostatic Field. Can. J. Phys., vol. 45, 1967, pp. 279.

90. Jackson, J. E.; and Kane, J. A.: Breakdown and Detuning of Transmitting Antennas in the Ionosphere. Upper Atmosphere Res. Report no. 36. U. S. Naval Res. Lab., (Washington, D. C.), 1959.

91. Kane, J. A.; Jackson, J. E.; and Whale, H. A.: RF Impedance Probe Measurements of Ionospheric Electron Densities. J. of Res. of the NBS – D. Radio Propagation, vol. 66D, no. 6, Nov.-Dec. 1962.

NASA Space Vehicle Design Criteria Monographs Now Issued

SP-8001	(Structures)	Buffeting During Launch and Exit, May 1964
SP-8002	(Structures)	Flight-Loads Measurements During Launch and Exit, December 1964
SP-8003	(Structures)	Flutter, Buzz, and Divergence, July 1964
SP-8004	(Structures)	Panel Flutter, May 1965
SP-8005	(Environment)	Solar Electromagnetic Radiation, June 1965
SP-8006	(Structures)	Local Steady Aerodynamic Loads During Launch and Exit, May 1965
SP-8007	(Structures)	Buckling of Thin-Walled Circular Cylinders, revised August 1968
SP-8008	(Structures)	Prelaunch Ground Wind Loads, November 1965
SP-8009	(Structures)	Propellent Slosh Loads, August 1968
SP-8010	(Environment)	Models of Mars Atmosphere (1967), May 1968
SP-8011	(Environment)	Models of Venus Atmosphere (1968), December 1968
SP-8012	(Structures)	Natural Vibration Modal Analysis, September 1968
SP-8013	(Environment)	Meteoroid Environment Model - 1969 (Near-Earth to Lunar Surface), March 1969
SP-8014	(Structures)	Entry Thermal Protection, August 1968
SP-8015	(Guidance and Control)	Guidance and Navigation for Entry Vehicles, November 1968
SP-8016	(Guidance and Control)	Effects of Structural Flexibility on Spacecraft Control Systems, April 1969
SP-8017	(Environment)	Magnetic Fields - Earth and Extraterrestrial, March 1969
SP-8018	(Guidance and Control)	Spacecraft Magnetic Torques, March 1969
SP-8019	(Structures)	Buckling of Thin-Walled Truncated Cones, September 1968
SP-8020	(Environment)	Mars Surface Models (1968), May 1969
SP-8021	(Environment)	Models of Earth's Atmosphere (120 to 1000 km), May 1969
SP-8023	(Environment)	Lunar Surface Models, May 1969
SP-8024	(Guidance and Control)	Spacecraft Gravitational Torques, May 1969
SP-8025	(Chemical Propulsion)	Solid Rocket Motor Metal Cases, June 1969
SP-8026	(Guidance and Control)	Spacecraft Star Trackers, July 1970
SP-8027	(Guidance and Control)	Spacecraft Radiation Torques, October 1969

SP-8028	(Guidance and Control)	Entry Vehicle Control, November 1969
SP-8029	(Structures)	Aerodynamic and Rocket-Exhaust Heating During Launch and Ascent, May 1969
SP-8031	(Structures)	Slosh Suppression, May 1969
SP-8032	(Structures)	Buckling of Thin-Walled Doubly Curved Shells, August 1969
SP-8033	(Guidance and Control)	Spacecraft Earth Horizon Sensors, December 1969
SP-8034	(Guidance and Control)	Spacecraft Mass Expulsion Torques, December 1969
SP-8035	(Structures)	Wind Loads During Ascent, June 1970
SP-8036	(Guidance and Control	Effects of Structural Flexibility on Launch Vehicle Control Systems, February 1970
SP-8037	(Environment)	Assessment and Control of Spacecraft Magnetic Fields, September 1970
SP-8038	(Environment)	Meteoroid Environment Model-1970 (Interplanetary and Planetary) October 1970
SP-8040	(Structures)	Fracture Control of Metallic Pressure Vessels, May 1970
SP-8046	(Structures)	Landing Impact Attenuation for Non-Surface-Planing Landers, April 1970

NASA-Langley, 1971 —— 13